Momentum transport in the free fluid-porous medium transition layer: the one-domain approach

Roel Hernandez-Rodriguez, Philippe Angot, Benoit Goyeau, J. Alberto Ochoa-Tapia

Journal Pre-proofs

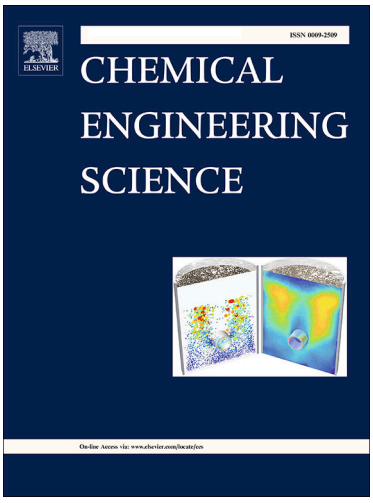

Momentum transport in the free fluid-porous medium transition layer: the one-domain approach

Roel Hernandez-Rodriguez, Philippe Angot, Benoit Goyeau, J. Alberto Ochoa-Tapia

PII: S0009-2509(21)00676-X
DOI: https://doi.org/10.1016/j.ces.2021.117111
Reference: CES 117111

To appear in: *Chemical Engineering Science*

Received Date: 9 April 2021
Revised Date: 2 July 2021
Accepted Date: 10 September 2021

Please cite this article as: R. Hernandez-Rodriguez, P. Angot, B. Goyeau, J.A. Ochoa-Tapia, Momentum transport in the free fluid-porous medium transition layer: the one-domain approach, *Chemical Engineering Science* (2021), doi: https://doi.org/10.1016/j.ces.2021.117111

Momentum transport in the free fluid-porous medium transition layer: the one-domain approach

Roel Hernandez-Rodriguez[a], Philippe Angot[b], Benoît Goyeau[c], J. Alberto Ochoa-Tapia[a,*]

[a] *División de Ciencias Básicas e Ingeniería, Universidad Autónoma Metropolitana-Iztapalapa. Av. San Rafael Atlixco 186, Col. Vicentina, 09340 CDMX, Mexico.*
[b] *Aix-Marseille Université, Institut de Mathématiques de Marseille, UMR-CNRS 7373, Centrale Marseille, 39 rue F. Joliot-Curie, 13453 Marseille cedex 13, France.*
[c] *Laboratoire EM2C, UPR-CNRS 288, Ecole Centrale-Supélec, Université Paris-Saclay, Grande Voie des Vignes F92-295 Châtenay-Malabry Cedex, France.*

Abstract

In this work, we consider the momentum transport of a incompressible fluid in a like Beavers and Joseph (1967) system. For this purpose, in the context of the volume averaging method, we use a one-domain approach (ODA). Thus, the momentum generalized transport equations (GTE), which are written in terms of position-dependent effective medium coefficients, are valid everywhere in the system and contains two Brinkman corrections in addition to a Darcy's term. The ODA predictions are tested against the results obtained from averaging the local profiles resulting from pore-scale simulations. One of the key points for solving the ODA remains on the prediction of the permeability, which in this work is obtained either by solving the associated local closure problem or from pore-scale profiles. Our analysis shows that the GTE for momentum transport accurately predicts the average velocity profiles everywhere in the system. To this end, the first and the second Brinkman's corrections, as well as a position-dependent intrinsic permeability tensor in Darcy's term must be included.

Keywords: momentum transport, one-domain approach, free flow/porous medium inter-region, local closure problem

1. Introduction

Momentum transport at a free flow/porous medium inter-region has been the object of intense research activity from the pioneering study by Beavers & Joseph (1967), where a Poiseuille flow over a permeable medium was considered. In fact, most of the theoretical and experimental

*Corresponding author
Email address: jaot@xanum.uam.mx (J. Alberto Ochoa-Tapia)

studies (see the recent state of the art in Angot et al. (2017)) concerning momentum transport have used this configuration in order to characterize velocity fields at the different scales of the inter-region.

From a macroscopic point of view, two main approaches to characterize the fluid flow in a coupled flow system can be found in the literature: *the two-domain approach (TDA)* and *the one-domain approach (ODA)*. In the TDA (see Fig. 1(b)), the free flow/porous medium system is treated as two continuous regions separated by a diving surface, and different equations are applied in each domain. In addition, such equations need to be coupled at the dividing surface through the use of appropriate boundary conditions. Beavers & Joseph (1967) considered a TDA, where the momentum in the free flow and porous regions are governed by the Stokes and Darcy equations, respectively. In addition, since these differential equations are not of the same order, an empirical slip boundary condition is introduced. This jump condition involves a dimensionless slip coefficient that depends on the microstructure of the inter-region. Several studies have focused on its experimental and theoretical determination (Beavers et al., 1970; Taylor, 1971; Richardson, 1971; Sahraoui & Kaviany, 1992).

The TDA has been significantly improved during the last two decades. In the context of the volume averaging method, using the Darcy-Brinkman equation instead of Darcy's law in the porous medium and assuming continuity of velocities at the interface, Ochoa-Tapia & Whitaker (1995a) derived a stress jump condition whose jump coefficient also depends on the microstructure of the inter-region (Goyeau et al., 2003). Chandesris & Jamet (2006, 2007, 2009) developed a matched asymptotic expansion method to show that jump conditions at the dividing surface both concern the velocity and the shear stress and that the jump coefficients do not only depend on the microstructure of the porous medium but also on the location of the dividing surface. The same conclusions have been recently drawn by using the volume averaging method (Valdés-Parada et al., 2013). In addition, the jump conditions have been recently generalized for multi-dimensional free flow/porous medium configurations (Angot et al., 2017). Other multidimensional boundary conditions have also been derived by using the multiscale homogenization method (Jäger et al., 2001; Jäger & Mikelić, 2009; Carraro et al., 2015; Zampogna & Bottaro, 2016; Lācis & Bagheri, 2017), which have been validated and calibrated for two-dimensional flows in different coupled free flow/porous medium systems (Rybak et al., 2020; Eggenweiler & Rybak, 2020).

On the other hand, in the ODA (see Fig. 1(a)), the free flow/porous medium system is viewed as a pseudo-continuum domain, and the transport is governed by generalized transport

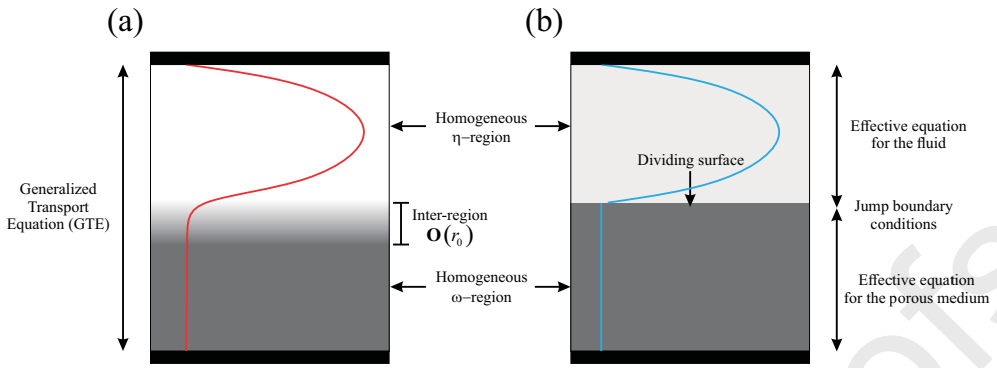

Figure 1: View of domains and velocity profiles in (a) the one-domain approach and (b) the two-domain approach.

equations (GTE) valid everywhere in the system. This approach has been applied, among others, by Caltagirone (1994); Angot et al. (1999); Bruneau & Mortazavi (2004, 2008); Bruneau et al. (2010); Hussong et al. (2011), but it is still not clear how the permeability in the inter-region should vary, thus different heuristic expressions for permeability has been commonly used (*e.g.*, Heaviside, linear, sinusoidal, error, or hyperbolic tangent function). However, there is no guarantee that such models can provide an accurate description of the fluid velocity in the homogeneous regions and mainly in the free flow/porous medium inter-region. In their works, Cimolin & Discacciati (2013) and Hussong et al. (2011) showed that even if the predictions a GTE in the homogeneous regions can be similar to those obtained from averaging the local fields or a TDA, the comparison near the interface can not be satisfactory. This exhibits the relevance of taking into account the correct spatial dependence of permeability everywhere in the system. In addition, it is unknown up to now how the spatial variations of effective coefficients are related to the size of the averaging volume used to derive the macroscopic equations, which can influence the comparison of theoretical predictions with experimental observations.

A formal derivation of the GTE for total mass and momentum transport has been done by using the volume averaging method (Ochoa-Tapia & Whitaker, 1995a; Valdés-Parada et al., 2007a). The resulting equations are free of length scale constraints and, therefore, valid everywhere in the system (*i.e.*, in the homogeneous regions and at the inter-region). This GTE is, in fact, a general form of the Darcy-Brinkman equation since the porosity and intrinsic permeability tensor are continuously position-dependent. Moreover, it interestingly includes a first but also a second Brinkman correction, where the latter arises due to the porosity variations in the inter-region. There are several attempts to validate this GTE, but they have not been able to provide satisfactory results (Ochoa-Tapia & Whitaker, 1995b). Some authors have suggested

that the second Brinkman correction can be neglected, arguing that its contribution is indirectly included through other terms in the equations (Chandesris & Jamet, 2006, 2007, 2009), although this has not been proven. Furthermore, since a satisfactory validation of the GTE has not been presented so far, the additional terms may be regarded just as a result of the up-scaling method used to derive the macroscopic equations.

From the above, including or not the additional terms in the GTE for momentum transport is crucial in the study of many processes of interest since erroneous predictions in the average velocity profiles can also introduce errors in the prediction of heat and mass transport in such systems. On the other hand, in many cases, the GTE is crucial for the derivation of the jump conditions that complete the TDA, and including or not the additional terms can determine an accurate prediction of the associated jump coefficients and as well as the position of the dividing surface. In this way, it is first necessary to derive a reliable GTE that allows to accurately describe the momentum transport between a free flow and a porous medium.

The aim of this work is to demonstrate that the ODA, where the GTE is derived by using the volume averaging method and with a detailed prediction of the spatial variations of the effective properties, is suitable to provide an accurate description of the momentum transport between a free flow region and a porous medium. We validate the GTE by comparing the average velocity profiles resulting from the solution of the ODA with those obtained from averaging pore-scale profiles arising from pore-scale simulations (PSS) in a free flow/porous medium system with different porous medium models.

Thus, this work is organized as follows. First, in Section 2, we present the free flow/porous medium system under consideration and the governing equations and boundary conditions for the total mass and momentum transport at the microscale. In addition, at the macroscale, we derive the unclosed form of the corresponding GTE, where in order to close them, we also derive and formally solve the associated local closure problem (LCP). After that, in Section 3, the closed form of the GTE and the spatial dependence of the permeability in the inter-region from the solution of the LCP are presented. Then, in Section 4, we compare and validate the average velocity profiles obtained from the solution of the ODA with those resulting from averaging the local velocity profiles. Later on, in Section 5, we predict the spatial dependence of the permeability by using the PSS, and we compare again the solution of the ODA with those resulting from averaging the local profiles. Moreover, the effect of the particle size variation near the porous boundary on the intrinsic permeability and the average velocity profiles is analyzed in Section 6. Finally, the corresponding discussion and the conclusions are drawn in Sections 7

and 8, respectively.

2. Pore-scale and macro-scale problems

2.1. Pore-scale problem

Let us consider the flow of a fluid phase ($\beta-$phase) through a channel bounded by two impermeable walls (*i.e.*, at the top and the bottom) and partially filled with a homogeneous porous medium made of a rigid solid phase ($\sigma-$phase), similar to the one used by Beavers & Joseph (1967), as shown in Fig. 2. The flow is assumed to be stationary, incompressible, fully developed, and for a particle Reynolds number less than the unity (*i.e.*, under a Stokes flow regime). Hereafter, the zone occupied by the porous medium, with a height of L_ω, will be referred to as the $\omega-$region and the zone of the free flow, with a height of L_η, will be referred to as the $\eta-$region. In this way, the local governing equations for total mass and momentum transport for a Newtonian fluid are given by

$$\nabla \cdot \mathbf{v}_\beta = 0 \quad \text{in the } \beta-\text{phase} \tag{1a}$$

$$\mathbf{0} = -\nabla p_\beta + \rho_\beta \mathbf{g} + \mu_\beta \nabla^2 \mathbf{v}_\beta \quad \text{in the } \beta-\text{phase} \tag{1b}$$

where $\mathbf{v}_\beta$ is the local velocity, p_β is the local pressure, μ_β is the dynamic viscosity, ρ_β is the density and $\mathbf{g}$ is the gravity vector. The Eqs. (1a) and (1b) must be solved subject to the non-slip boundary condition at the solid-fluid interface ($\mathscr{A}_{\beta\sigma,M}$) contained in the porous medium, which is given by

$$\mathbf{v}_\beta = \mathbf{0} \quad \text{at} \quad \mathscr{A}_{\beta\sigma,M} \tag{1c}$$

This boundary condition must also be satisfied at the surface of the impermeable walls that bound the channel. In addition, to complete the statement of the boundary value problem, it is necessary to provide the boundary conditions at entrances and exits of the system ($\mathscr{A}_{\beta e,M}$). In this case, the flow in the η and $\omega-$regions is driven by the same constant pressure drop in the horizontal direction (*i.e.*, $x-$direction).

As mentioned above, to avoid the high computational cost required for the solution of the pore-scale problem, as well as the treatment of the resulting information, the ODA can be used. For the problem given by Eqs. (1), the derivation of the corresponding GTE for the ODA, using the method of volume averaging (Whitaker, 1999), was first carried out by Ochoa-Tapia & Whitaker (1995a) and more recently by Valdés-Parada et al. (2007a). This latter work also provided the associated LCP to predict the spatial variations of the intrinsic permeability

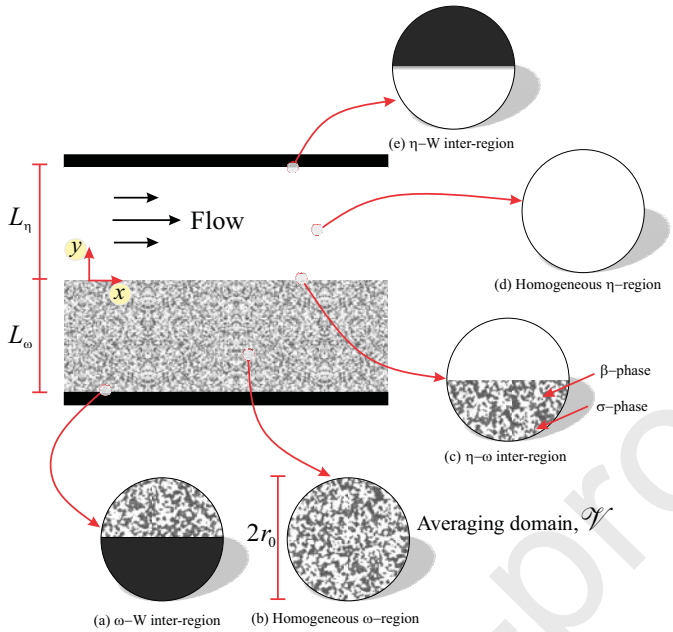

Figure 2: Sketch of the channel partially filled with a porous medium and samples in the two homogeneous regions ((b) homogeneous porous medium and (d) homogeneous free flow) and in the inter-regions ((a) impermeable wall/porous medium, (c) free flow/porous medium and (e) free flow/impermeable wall).

tensor. Therefore, the main originalities of our work consist of the strict validation of the LCP and the additional terms involved in the GTE of such methodology. For such reason, in the following section, we revisit the derivation of the GTE for total mass and momentum transport, and we predict the effective coefficients from both the solution of the LCP and the pore-scale information obtained by performing a PSS. For conciseness, we only present here those steps of the derivation where modifications are required.

2.2. Averaging

The first step of the development is to define an averaging volume of size V and locus $\mathscr{V}(\mathbf{x})$ at every point of the system, as those shown in Fig. 2. Notice that $\mathscr{V}$ may be located in the homogeneous regions and the inter-regions, so it may contain the β and $\sigma-$phases but also the solid phase of the upper or lower wall. In this way, in terms of the averaging domain, the superficial averaging operator for a local variable ψ_β defined in the $\beta-$phase can be written as

$$\langle \psi_\beta \rangle|_{\mathbf{x}} = \frac{1}{V} \int\limits_{\mathbf{y}_\beta \in \mathscr{V}_\beta(\mathbf{x})} \psi_\beta|_{\mathbf{x}+\mathbf{y}_\beta} \, dV \tag{2}$$

which is related to the intrinsic average by

$$\langle \psi_\beta \rangle|_{\mathbf{x}} = \varepsilon_\beta(\mathbf{x}) \langle \psi_\beta \rangle^\beta \Big|_{\mathbf{x}} \tag{3}$$

where $\varepsilon_\beta(\mathbf{x}) = V_\beta(\mathbf{x})/V$ is the volume fraction of the $\beta-$phase contained in the averaging volume. Notice that the value of ε_β is reduced to the porosity of the bulk of the porous medium ($\varepsilon_{\beta\omega}$) in the homogeneous $\omega-$region and to 1 in the homogeneous $\eta-$region. In the above equations, the vector $\mathbf{x}$ locates the position of the centroid of the averaging volume relative to an arbitrary reference system, the vector $\mathbf{r}_\beta = \mathbf{x} + \mathbf{y}_\beta$ locates points of the $\beta-$phase contained in the averaging volume relative to the same reference system, and the vector $\mathbf{y}_\beta$ locates points in the $\beta-$phase contained in the averaging volume but relative to the vector $\mathbf{x}$.

2.3. Generalized transport equations

Now, let us apply the superficial averaging operator given by Eq. (2) to Eqs (1a) and (1b), where by using the spatial averaging theorem (Howes & Whitaker, 1985), incorporating the non-slip boundary condition given by Eq. (1c) and after of some algebraic manipulations, yields

$$\nabla \cdot \langle \mathbf{v}_\beta \rangle|_{\mathbf{x}} = 0 \tag{4a}$$

$$\begin{aligned} \mathbf{0} = -\nabla \langle p_\beta \rangle^\beta \Big|_{\mathbf{x}} + \rho_\beta \mathbf{g} + \varepsilon_\beta^{-1}(\mathbf{x}) \mu_\beta \nabla^2 \langle \mathbf{v}_\beta \rangle|_{\mathbf{x}} \\ - \mu_\beta \varepsilon_\beta^{-1}(\mathbf{x}) \nabla \varepsilon_\beta \cdot \nabla \left(\varepsilon_\beta^{-1}(\mathbf{x}) \langle \mathbf{v}_\beta \rangle \Big|_{\mathbf{x}} \right) + \mathbf{f}_\beta(\mathbf{x}) \end{aligned} \tag{4b}$$

Here μ_β and ρ_β were assumed to be constant within the averaging volume. The details of the derivation of these equations can be seen elsewhere (Ochoa-Tapia & Whitaker, 1995a; Valdés-Parada et al., 2007a). In addition, in the above equations we have introduced the position-dependent vector $\mathbf{f}_\beta(\mathbf{x})$ defined as

$$\mathbf{f}_\beta(\mathbf{x}) = \frac{1}{V_\beta(\mathbf{x})} \int_{\mathscr{A}_{\beta\sigma}(\mathbf{x})} \mathbf{n}_{\beta\sigma} \cdot \left[-\mathbf{I} \left(p_\beta|_{\mathbf{r}_\beta} - \langle p_\beta \rangle^\beta \Big|_{\mathbf{x}} \right) + \mu_\beta \left(\nabla \mathbf{v}_\beta|_{\mathbf{r}_\beta} - \nabla \langle \mathbf{v}_\beta \rangle^\beta \Big|_{\mathbf{x}} \right) \right] dA \tag{5}$$

where $\mathscr{A}_{\beta\sigma}(\mathbf{x})$ denotes the solid-fluid interfaces contained in the averaging volume. Notice that Eq. (4a) resembles its pore-scale counterpart given by Eq. (1a). However, in Eq. (4b) this is only true for the first three terms, where the last of them is a macroscopic viscous term known in the literature as the first Brinkman correction with the effective viscosity give by $\mu_{eff} = \mu_\beta/\varepsilon_\beta(\mathbf{x})$. Furthermore, two new terms appear as result of the averaging procedure: the term $\mu_\beta \varepsilon_\beta^{-1}(\mathbf{x}) \nabla \varepsilon_\beta \cdot \nabla \left(\varepsilon_\beta^{-1}(\mathbf{x}) \langle \mathbf{v}_\beta \rangle \Big|_{\mathbf{x}} \right)$ is referred to as the second Brinkman correction that

captures other macroscopic viscous forces due to the spatial variations of $\varepsilon_\beta(\mathbf{x})$ and the term $\mathbf{f}_\beta(\mathbf{x})$ is referred to as the friction term that captures all the resistances offered by the solid phase to the fluid motion (Ochoa-Tapia & Whitaker, 1995a).

It is worth noting that, at this point in the derivation of Eqs. (4), no length-scale constraint has been imposed, so they are valid everywhere in the free flow/porous medium system. The Eqs. (4) are thus the exact generalized transport equations (GTE) for total mass and momentum transport (Ochoa-Tapia & Whitaker, 1995a,b; Valdés-Parada et al., 2007a). However, Eq. (4b) still depends on the pore-scale problem given by Eqs. (1) due to the vector $\mathbf{f}_\beta(\mathbf{x})$, so it is more complex than the original problem. This difficulty has often been addressed in the literature by postulating the form of the vector $\mathbf{f}_\beta(\mathbf{x})$, and then evaluating the consequences of such a choice. For instance, for a Stokes flow, the vector $\mathbf{f}_\beta(\mathbf{x})$ is often replaced by the Darcy's equation, while for an inertial flow, it is commonly replaced by Ergun's equation. These approaches are the most widely used in modeling of fluid flows over porous media (Beckermann et al., 1988; Khalili et al., 1998; Gobin et al., 1998, 2005; Jiménez-Islas et al., 2009) but also through fixed bed reactors (Vafai & Tien, 1981, 1982; Cheng et al., 1991; Das et al., 2018; George et al., 2021). Nevertheless, in these approaches there is no guideline to predict the spatial variations of permeability and the volume fraction, leading to the usage of empirical expressions for it.

In order to overcome this difficulty, it is necessary to derive and formally solve an associated LCP. To this end, let us introduce the spatial decomposition of a local variable ψ_β, in terms of its intrinsic average $\langle\psi_\beta\rangle^\beta$ and local deviations $\tilde{\psi}_\beta$, as follows (Gray, 1975)

$$\psi_\beta|_{\mathbf{r}_\beta} = \langle\psi_\beta\rangle^\beta\Big|_{\mathbf{r}_\beta} + \tilde{\psi}_\beta\Big|_{\mathbf{r}_\beta} \tag{6}$$

This allows us to write Eq. (5) as

$$\mathbf{f}_\beta(\mathbf{x}) = \frac{1}{V_\beta(\mathbf{x})}\int_{\mathscr{A}_{\beta\sigma}(\mathbf{x})} \mathbf{n}_{\beta\sigma}\cdot\left[-\mathbf{I}\left(\tilde{p}_\beta|_{\mathbf{r}_\beta} + \Delta\langle p_\beta\rangle^\beta\right) + \mu_\beta\left(\nabla\tilde{\mathbf{v}}_\beta|_{\mathbf{r}_\beta} + \Delta\langle\mathbf{v}_\beta\rangle^\beta\right)\right]dA \tag{7}$$

where the following definition has been introduced

$$\Delta\langle\psi_\beta\rangle^\beta = \langle\psi_\beta\rangle^\beta\Big|_{\mathbf{r}_\beta} - \langle\psi_\beta\rangle^\beta\Big|_{\mathbf{x}} \quad \text{for} \quad \psi_\beta = \mathbf{v}_\beta, p_\beta \tag{8}$$

Now Eq. (4b) is an unclosed average equation valid everywhere, since Eq. (7) involves two kind of dependent variables (*i.e.*, the averages and the deviations) and only one set of governing equations. In this way, it is necessary to find expressions for the local velocity $\tilde{\mathbf{v}}_\beta$ and local pressure $\tilde{p}_\beta$ deviations in terms of the average quantities, which is a procedure known as *the closure problem*. The details of the derivation and the formal solution of the deviations problem

are provided in Appendix A. Here it is enough to mention the formal solution for the local velocity and local pressure deviations can be written as (Valdés-Parada et al., 2007a, 2009a)

$$\tilde{\mathbf{v}}_\beta = \mathbf{B}_\beta \cdot \langle \mathbf{v}_\beta \rangle^\beta \Big|_{\mathbf{x}} \tag{9a}$$

$$\tilde{p}_\beta = \mu_\beta \mathbf{b}_\beta \cdot \langle \mathbf{v}_\beta \rangle^\beta \Big|_{\mathbf{x}} \tag{9b}$$

where the vector $\mathbf{b}_\beta$ and the second order tensor $\mathbf{B}_\beta$ are referred to as local closure variables, which can be predicted from the solution of the associated LCP reported in Appendix A. It is worth mentioning that the formal solution for the local deviations are valid provided the length-scale constraints given by $r_0/L \ll 1$, $r_0^2/L^2 \ll 1$ and $\ell^2/(r_0 L) \ll 1$ are satisfied (Valdés-Parada et al., 2007a, 2009a). Here ℓ is the largest characteristic length associated to the pore-scale, r_0 is characteristic size of the averaging volume, and L the smallest characteristic length associated to the macroscale. In addition, it should be noticed that, under the same length-scale constraints, the term $\mathbf{f}_\beta(\mathbf{x})$ given by Eq. (7) can be reduced to

$$\mathbf{f}_\beta(\mathbf{x}) = \frac{1}{V_\beta(\mathbf{x})} \int_{\mathscr{A}_{\beta\sigma}(\mathbf{x})} \mathbf{n}_{\beta\sigma} \cdot \left[-\mathbf{I} \tilde{p}_\beta \big|_{\mathbf{r}_\beta} + \mu_\beta \nabla \tilde{\mathbf{v}}_\beta \big|_{\mathbf{r}_\beta} \right] dA \tag{10}$$

3. Closed generalized transport equation

To obtain the closed form of the GTE for momentum transport, let us introduce the formal solution for the deviations given by Eqs. (9) into Eq. (10), which leads to express the Eq. (4b) as

$$\begin{aligned} \mathbf{0} = -\nabla \langle p_\beta \rangle^\beta \Big|_{\mathbf{x}} + \rho_\beta \mathbf{g} + \varepsilon_\beta^{-1}(\mathbf{x}) \mu_\beta \nabla^2 \langle \mathbf{v}_\beta \rangle \big|_{\mathbf{x}} \\ - \mu_\beta \varepsilon_\beta^{-1}(\mathbf{x}) \nabla \varepsilon_\beta \cdot \nabla \left(\varepsilon_\beta^{-1}(\mathbf{x}) \langle \mathbf{v}_\beta \rangle \Big|_{\mathbf{x}} \right) \\ - \mu_\beta \varepsilon_\beta(\mathbf{x}) \ \mathbf{K}_\beta^{-1}(\mathbf{x}) \cdot \langle \mathbf{v}_\beta \rangle^\beta \Big|_{\mathbf{x}} \end{aligned} \tag{11}$$

where the term $\mathbf{f}_\beta(\mathbf{x})$ is now written as a Darcy's term with a position-dependent intrinsic permeability tensor $\mathbf{K}_\beta(\mathbf{x})$. This coefficient is defined in terms of the local closure variables according to the following expression

$$-\varepsilon_\beta(\mathbf{x}) \mathbf{K}_\beta^{-1}(\mathbf{x}) = \frac{1}{V_\beta(\mathbf{x})} \int_{\mathscr{A}_{\beta\sigma}(\mathbf{x})} \mathbf{n}_{\beta\sigma} \cdot (-\mathbf{I}\mathbf{b}_\beta + \nabla \mathbf{B}_\beta) \, dA \tag{12}$$

Thus, to compute the spatial variations of the permeability tensor it is necessary to solve the associated LCP given by Eqs. (A.3), in a periodic representative domain of the free flow/porous

medium boundary. Notice that $\mathbf{K}_{\beta}^{-1}(\mathbf{x})$ reduces to the inverse of the permeability of the bulk of the porous medium $\mathbf{K}_{\beta\omega}^{-1}$ in the homogeneous $\omega-$region and reduces to zero in the homogeneous $\eta-$region. The value of $\mathbf{K}_{\beta\omega}$ can also be computed by solving the associated LCP in a unit cell of the bulk of the porous medium. In that case, for the local closure variables, periodic boundary conditions need to be imposed at all boundaries (Whitaker, 1999).

Hence Eqs. (4a) and (11) are respectively the closed GTE for total mass and momentum transport and they constitute the base of the ODA. It is worth stressing that Eq. (11) is valid in the $\eta - \omega$ inter-region as long as the constrains given by Eq. (A.2) are satisfied. Goyeau et al. (2003) considered a simplified form of Eq. (11) as the GTE for momentum transport of an ODA, where the effective medium coefficients were heuristic functions of position.

Solution of the local closure problem

From the above, to solve the ODA, the spatial variations of the effective medium coefficients must be already known. In this sense, the spatial variation of $\mathbf{K}_{\beta}$ in the $\eta - \omega$ inter-region can be predicted from the solution of the associated LCP. To this end, the periodic representative domain of the free flow/porous medium boundary shown in Fig. 3 was considered. The geometry of the porous medium consists of a periodic array of a two-dimensional unit cell with a centered circular particle. Thus, a rectangular domain with a height $h = h_{\omega} + h_{\eta}$ and a width equal to the side length of a unit cell ℓ was enough to take as the solution domain for the LCP. It is worth mentioning that h must be large enough to include the $\eta - \omega$ inter-region and that the permeability predictions at the top and bottom correspond to those of the homogeneous regions.

Before moving on, it should be noticed that to predict the permeability by using Eqs. (12), it is necessary to define the shape and size of an averaging volume. To this end, a cross-section area equal to $2r_0\ell$ was used (see Fig. 3). For simplicity, in all the calculations, the ratio r_0/ℓ was chosen to be an integer number. It is pertinent to point out that the locus chosen here must be consistent with those used for averaging the local fields resulting from the PSS, as shown below and by Hernandez-Rodriguez et al. (2020). Using the same size and geometry of the averaging volume avoids introducing additional uncertainty sources when the average velocity profiles obtained from the solution of ODA are compared with those resulting from averaging the local velocity profiles.

The LCP given by Eqs. (A.5), obtained after a change of variable as suggested by Whitaker (1999), was numerically solved using the finite element software COMSOL Multiphysics 5.2. A free triangular unstructured mesh was employed, and the direct PARADISO solver was chosen.

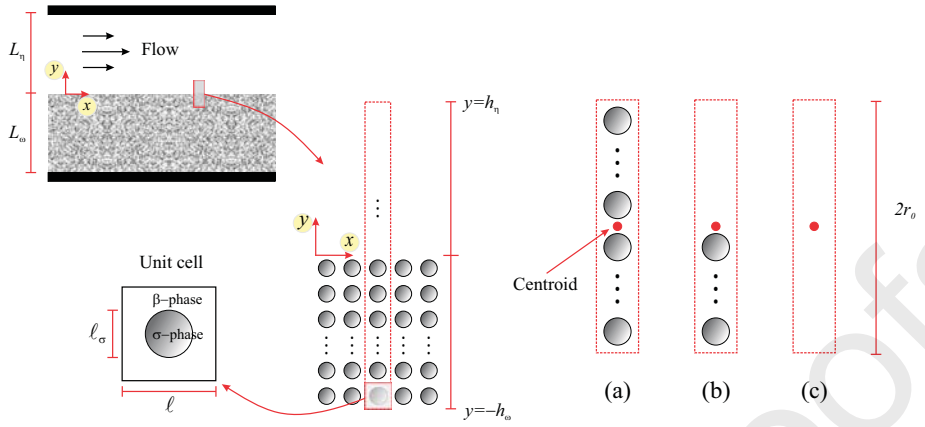

Figure 3: Periodic representative domain of the free flow/porous medium boundary used for the solution of the LCP and samples at (a) $y = -r_0$, (b) $y = 0$ and (c) $y = +r_0$. The porous medium is made of a periodic array of a unit cell with a centered circular particle.

An adaptive mesh refinement technique was used to ensure that all the results were independent of the number of computational nodes. Here, the heights of the free-flow and the porous medium regions contained in the solution domain are related to the characteristic size of the averaging volume. They must be at least equal to $h_\eta = 2r_0$ and $h_\omega = 2r_0 + 3\ell$. Hence, the position of the centroid of the samples is constrained to the positions given by $-(3\ell + r_0) \leq y \leq +r_0$. Then, with the closure variables fields, the spatial variations of permeability were predicted using Eq. (A.6). It should be noticed that, because in the system under consideration, the flow is assumed to be fully developed, the only needed component of the permeability tensor to predict the average velocity is the $xx-$component (*i.e.*, $K_\beta = \mathbf{e}_x \cdot \mathbf{K}_\beta \cdot \mathbf{e}_x$). Besides, due to the periodicity of the porous medium geometry in the horizontal direction, the spatial variations of the permeability take place only along the vertical axis (*i.e.*, $y-$direction).

In Fig. 4 we show the spatial variations of K_β^{-1} in the $\eta-\omega$ inter-region taking different sizes of the averaging volume for two values of $\varepsilon_{\beta\omega}$. From these results, one can observe that K_β^{-1} undergoes abrupt changes between its value in one homogeneous region to the other. Notice that K_β^{-1} reaches the value of $K_{\beta\omega}^{-1}$ when the averaging volume is located at $y \approx -(\ell + r_0)$ and zero when the averaging volume is located at $y \approx +r_0$. Thus, the zone of changes of permeability predicted from the solution of the LCP is constrained to the positions given by $-(\ell + r_0) \leq y \leq +r_0$, and that it has a thickness equal to $2r_0 + \ell$. The value of the lower limit is more evident when r_0 tends to the size of the side length of a unit cell ℓ. In addition, one can appreciate that K_β^{-1} decreases as the value of r_0 is increased, and it increases as the value of

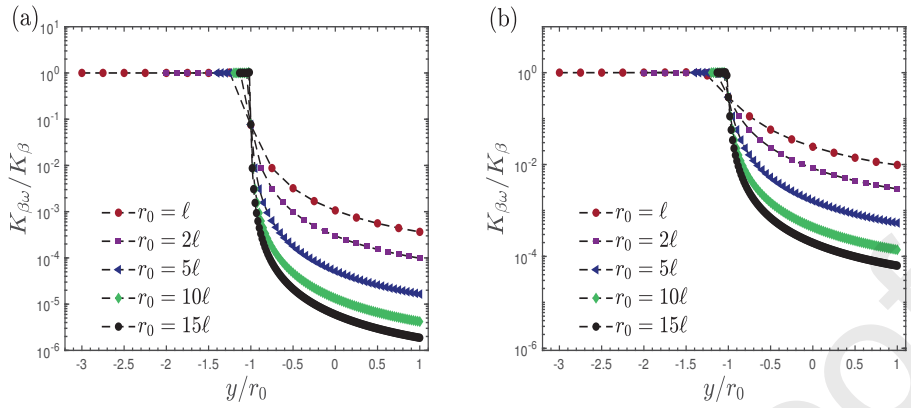

Figure 4: Spatial variations of permeabilities ratio $K_{\beta\omega}/K_\beta\,(Y)$ in the free flow/porous medium inter-region. The porous medium model is made of a periodic array of a unit cell with a centered circle. All the calculations are obtained from the solution of the LCP taking different values of r_0 for two values of $\varepsilon_{\beta\omega}$: (a) 0.4 and (b) 0.8.

$\varepsilon_{\beta\omega}$ is increased. All these observations contrast sharply with those presented by Valdés-Parada et al. (2009a); Aguilar-Madera et al. (2011), where the strategy used to solve the LCP led them to obtain smoothed permeability predictions for porous medium models consisting of a periodic array of two and three-dimensional unit cells with non-touching squares and cubes, respectively.

Finally, other needed coefficient for the ODA solution is the fluid volume fraction ε_β. This can be obtained by applying Eq. (2) for $\psi_\beta = 1$ along the vertical direction of the domain shown in Fig. 3. As mentioned above, the corresponding values of ε_β in the bulk of the porous medium and free flow are $\varepsilon_{\beta\omega}$ and 1, respectively. However, in the $\eta - \omega$ inter-region, it exhibits an oscillatory behavior tending to a straight line as the value of r_0 increases. For the geometry of the porous medium here considered, the zone of changes is restricted to the positions given by $-r_0 \leq y \leq +r_0$, which does not necessarily coincide with the zone of changes of K_β predicted from the solution of the LCP. It should be noticed that it is possible to derive an algebraic expression, that includes the floor function, to describe the dependence of ε_β on y. However, for practical purposes, a linear interpolation between $\varepsilon_{\beta\omega}$ and 1 can be used. This was tested by solving the ODA using the exact and linear predictions of ε_β. The differences between both average velocity profiles were negligible.

In the following section, for the system like the one used by Beavers & Joseph (1967), we compare the average velocity profiles obtained from solving an ODA written in terms of Eqs. (11) and those obtained from averaging the local velocity profiles resulting from a PSS.

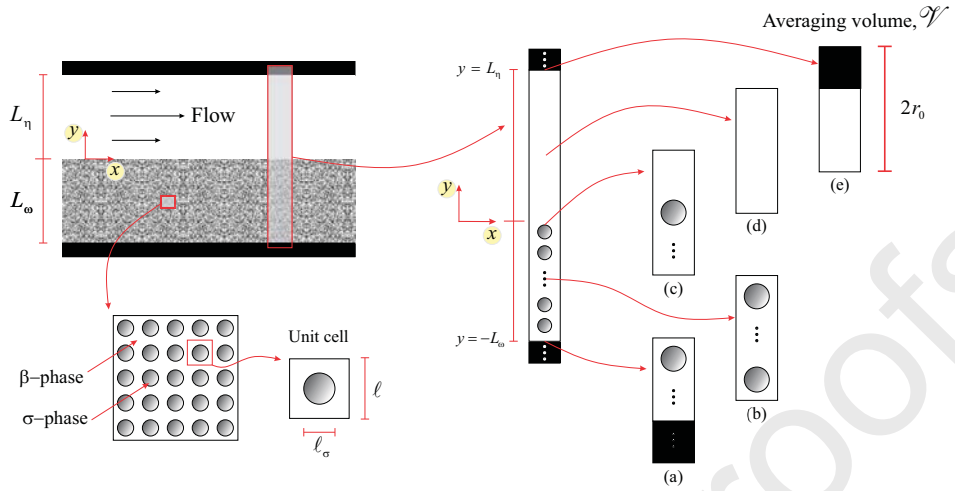

Figure 5: Periodic domain for the solution of the microscopic problem and samples in different positions of the system: (a) impermeable wall/porous medium inter-region, (b) homogeneous porous medium, (c) free flow/porous medium inter-region, (d) homogeneous free flow region, and (e) free flow/impermeable wall.

4. ODA solution I: GTE in terms of K_β obtained from the local closure problem

Now that the GTE for momentum transport is already closed, it is necessary to evaluate its predictive capabilities. To this end, in this section, we compare the average velocity profiles resulting from the solution of the ODA with those resulting from averaging, using an averaging volume of characteristic size r_0, the local velocity profiles obtained by performing a PSS.

For purposes of this comparison, a channel partially filled with a porous medium (see Fig. 2) consisting of a free flow and porous medium regions, respectively, with the heights of $L_\eta = 10^3\ell$ and $L_\omega = 10^2\ell$ was considered. Thus the free flow/porous medium system has a total height of $L_T = L_\eta + L_\omega = 1.1 \times 10^3\ell$. This satisfies the disparity of characteristic lengths given by $\ell \ll L$. For the sake of consistency with the effective medium coefficients predicted in the previous section, at the microscale, a porous medium region made of a periodic array of a two-dimensional unit cell with a centered circular particle was used. With this mind, the PSS consist of numerically solving the pore-scale problem given by Eq. (1), along with the non-slip boundary condition at the top and the bottom impermeable walls, everywhere in the system. However, due to the fully developed flow assumption and the periodic nature of the porous medium, a periodic domain of the whole channel with a height L_T and a width ℓ was enough to take as the solution domain for the PSS, such as the one shown in Fig. 5. To generate the

flow a dimensionless average pressure drop given by $C = \left(\ell^3 \rho_\beta \Delta \langle p_\beta \rangle^\beta\right) / \left(L \mu_\beta^2\right) = 10^{-5}$ was imposed. With this value of C the Reynolds number of the porous medium region, based on the particle size, is restricted to $Re_p \ll 1$, while the Reynolds number of the free flow region, based on the height of such a region, satisfies that $Re_\eta \leq 1250$. Finally, periodic boundary conditions for the local pressure deviations and local velocity were enforced in the x and z directions. The details of the numerical solution can be seen elsewhere (Hernandez-Rodriguez et al., 2020).

In this way, the PSS was carried out using a strategy similar to that used to solve the LCP. Once the local velocity profiles were available, they were substituted into Eq. (2) to obtain the superficial average velocity profiles in the whole system. To this end, the shape and size of the averaging volume were chosen to be equal to those used to compute the spatial variations of the effective medium coefficients. It is worth noting that the local fields does not depend on the size of the averaging volume while the average quantities do.

On the other hand, at the macroscale, the governing equations for the system under consideration are given by Eqs. (4a) and (11). For simplicity, it is convenient to write them in dimensionless form by using the dimensionless variables given by

$$X = \frac{x}{\ell}; \quad Y = \frac{y}{\ell}; \quad \langle \mathbf{u} \rangle = \frac{\langle \mathbf{v}_\beta \rangle \ell \rho_\beta}{\mu_\beta}; \quad \langle p \rangle^\beta = \frac{\ell^2 \rho_\beta (\langle p_\beta \rangle^\beta + \rho_\beta y g)}{\mu_\beta^2}; \quad \mathbf{K}_\beta^* = \frac{\mathbf{K}_\beta}{\ell^2} \tag{13}$$

Thus the GTE for total mass and momentum transport take the following form

$$\nabla \cdot \langle \mathbf{u} \rangle = 0 \tag{14a}$$

$$\mathbf{0} = -\nabla \langle p \rangle^\beta + \varepsilon_\beta^{-1}(\mathbf{X}) \nabla^2 \langle \mathbf{u} \rangle - \varepsilon_\beta^{-1}(\mathbf{X}) \nabla \varepsilon_\beta \cdot \nabla \left(\varepsilon_\beta^{-1}(\mathbf{X}) \langle \mathbf{u} \rangle \right) - \mathbf{K}_\beta^{*-1}(\mathbf{X}) \cdot \langle \mathbf{u} \rangle \tag{14b}$$

where ∇ now represents the dimensionless differential operator. However, since the flow is fully developed and unidirectional, similar to the system used by Beavers & Joseph (1967), the only non-zero component of the average velocity vector is the horizontal one to the surface of the porous medium (*i.e.*, the $x-$component). Thus taking the scalar product of Eqs. (14) with the unit vector in the $x-$direction (*i.e.*, $\mathbf{e}_x$), yields

$$0 = -\frac{d\langle p \rangle^\beta}{dX} + \varepsilon_\beta^{-1}(Y) \frac{d^2 \langle u \rangle}{dY^2} - \varepsilon_\beta^{-1}(Y) \frac{d\varepsilon_\beta}{dY} \frac{d}{dY} \left(\varepsilon_\beta^{-1}(Y) \langle u \rangle \right) - K_\beta^{*-1}(Y) \langle u \rangle \tag{15}$$

where $\langle u \rangle = \langle \mathbf{u} \rangle \cdot \mathbf{e}_x$ and $K_\beta^{*-1}(Y) = \mathbf{e}_x \cdot \mathbf{K}_\beta^{*-1}(\mathbf{X}) \cdot \mathbf{e}_x$. In addition, to complete the statement of the macroscopic problem, the following boundary conditions at the top and the bottom of

the channel are imposed

$$\langle u\rangle = 0 \quad \text{at} \quad Y = (L_\eta + r_0)/\ell \tag{16a}$$

$$\langle u\rangle = \langle u\rangle_{\omega,\infty} \quad \text{at} \quad Y = -(L_\omega - r_0)/\ell \tag{16b}$$

where $\langle u\rangle_{\omega,\infty}$ is the average velocity in the bulk of the porous medium (*i.e.*, Darcy's velocity) which is given by $\langle u\rangle_{\omega,\infty} = -K^*_{\beta\omega} d\langle p\rangle^\beta_\omega / dX$. On the one hand, notice that instead of using the non-slip boundary condition at the lower impermeable wall (*i.e.*, at $y = -L_\omega$), the velocity existing in the bulk of the porous medium was imposed at $y = -L_\omega + r_0$. This is to avoid unnecessary calculations since sufficiently below the beginning of the porous medium, the local velocity fields are periodic, and therefore Darcy's velocity is reached. In fact, in previous work, we have found that the bulk conditions are reached at a distance $\delta_B \approx r_0 + 3\ell$ below the surface of the porous medium (Hernandez-Rodriguez et al., 2020). On the other hand, notice that the upper boundary condition was located inside of the upper impermeable wall. This is because, in the average sense, the average velocity is not necessarily zero at $y = L_\eta$ since, in that position, the averaging domain still contains portions of the $\eta-$region, as shown by Ochoa-Tapia et al. (2017). However, the above is only for purposes of the ODA solution, so that the results will be presented only from the position of the bulk of the porous medium (*i.e.*, $y = -L_\omega + r_0$) up to the upper impermeable wall (*i.e.*, $y = L_\eta$). Finally, due to the type of flow and experimental configuration considered by Beavers & Joseph (1967), it is reasonable to assume that the macroscopic pressure drop is given by

$$\frac{d\langle p\rangle^\beta}{dX} = \frac{d\langle p\rangle^\beta_\eta}{dX} = \frac{d\langle p\rangle^\beta_\omega}{dX} \tag{17}$$

In this way, the ODA consist of the GTE for the momentum transport given by Eq. (15), which is subject to the boundary conditions given by Eqs. (16). With this in mind, due to the position dependence of the effective medium coefficients (porosity and permeability), the ODA was numerically solved. To this end, a finite difference scheme to discretize the governing equation and a Gaussian-elimination method to solve the resulting algebraic equations were used. Standard tests of convergence and uniqueness were performed in order to guarantee the reliability of the numerical results.

In Fig. 6 we plot the average velocity profiles of the free flow/porous medium system obtained from both solving the ODA and averaging the local velocity fields resulting from the PSS taking different values of r_0 for $\varepsilon_{\beta\omega} = 0.4$. The intrinsic average velocity profiles are reported as follows

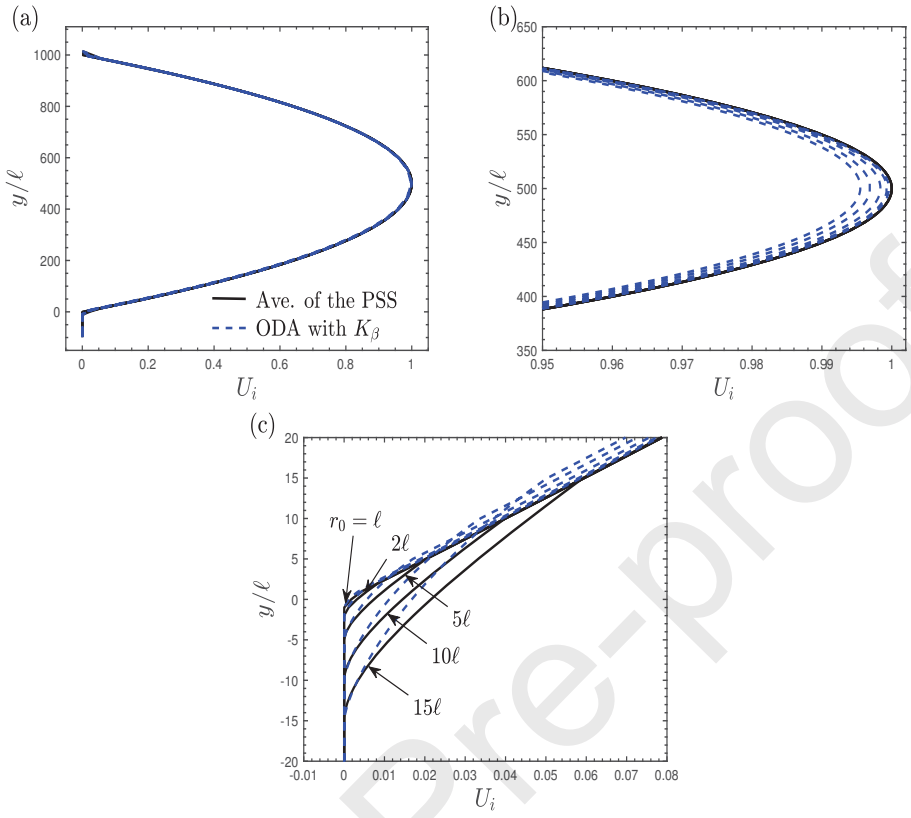

Figure 6: Comparison of intrinsic average velocity profiles in the channel partially filled with a porous medium obtained from averaging the PSS and ODA solution (with K_β predicted from the solution of the LCP) using different values of r_0 for $\varepsilon_{\beta\omega} = 0.4$. The velocity profiles are (a) in the whole channel, (b) around the maximum velocity and (c) in $\eta - \omega$ inter-region.The porous medium model consist of a periodic array of a unit cell with a centered circle. In all the calculations we used $L_\eta = 10^3\ell$ and $L_\omega = 10^2\ell$.

$$U_i = \frac{\langle u \rangle_i^\beta}{max(\langle u \rangle_{PSS}^\beta)}; \qquad i = PSS, ODA \tag{18}$$

A first assessment of the results can be obtained from Fig. 6(a), where the velocity profiles in the whole channel are presented. From this result, one can observe that the velocity profiles obtained from the ODA are similar to those obtained from averaging the local fields. However, the amplifications plotted in Figs. 6(b) and 6(c) show that the ODA predictions exhibit some deviations around the maximum velocity and in the free fluid/porous medium inter-region, respectively. These deviations are larger in the free flow/porous medium inter-region than those

Table 1: Relative error percentage of the ODA, with K_β predicted from the solution of the LCP, with respect to the average of the local fields, to predict the average velocity profile in the free fluid/porous medium inter-region for several values of r_0 and two values of $\varepsilon_{\beta\omega}$.

	centered circle	
r_0/ℓ	$\varepsilon_{\beta\omega} = 0.4$	$\varepsilon_{\beta\omega} = 0.8$
1	21.47	19.15
2	21.13	17.95
5	22.52	17.26
10	23.33	16.41
15	23.73	15.67

around the maximum velocity. Notice that the deviations seem to increase as the r_0 value is increased and when the averaging volume moves from the position located at $y = -r_0$ to that located at $y = +r_0$.

In order to quantify the predictive capabilities of the ODA, we computed the relative error percentage of the ODA to describe the average velocity profile in the $\eta-\omega$ inter-region according to the following expression

$$\text{Error}_1\ \% = \frac{100}{2r_0/\ell} \int_{Y=-r_0/\ell}^{Y=+r_0/\ell} \frac{\left|\langle u\rangle^\beta_{PSS} - \langle u\rangle^\beta_{ODA}\right|}{\langle u\rangle^\beta_{PSS}} dY \tag{19}$$

In Table 1 we present the values of $\text{Error}_1\%$ as function of r_0 for two values of $\varepsilon_{\beta\omega}$. These results are for the porous medium made of the unit cell shown in Fig. 5. As one can observe for $\varepsilon_{\beta\omega} = 0.4$ the relative error percentage is $22\pm$ 2 %. On the other hand, for $\varepsilon_{\beta\omega} = 0.8$ the relative percentage error decreases until $16\pm$ 2 %. This can be attributed to the fact that when porosity increases, flow resistances also decrease, and therefore, the accuracy of the LCP increases. These results suggest that the use of the LCP for permeability prediction may be restricted to high enough values of $\varepsilon_{\beta\omega}$.

To conclude this section, as indicated by Hernandez-Rodriguez et al. (2020), when the inequality given by $\ell \ll L_\eta$ is satisfied, one can expect that the errors in the predictions of the average velocity in the inter-region will not have significant effects on those located approximately in the middle of the free-flow region. To analyze this, we introduced the relative percentage error of the ODA to predict the maximum average velocity with respect to the average of the

local fields, as follows

$$\text{Error}_2\ \% = 100\frac{\left|\langle u\rangle^{\beta}_{PSS} - \langle u\rangle^{\beta}_{ODA}\right|}{\langle u\rangle^{\beta}_{PSS}} \tag{20}$$

In Table 2 we show the values of Error_2 % as function of r_0 for two values of $\varepsilon_{\beta\omega}$. In general, one can observe that in all cases, the error is lower than $\mathbf{O}(10^{-2})$. Thus one can confirm that the errors in the velocity profiles of the free fluid/porous medium inter-region introduced in the ODA, when K_β is obtained from the solution of the LCP, do not significantly affect the predictions of the maximum velocity in the free flow region.

From the above, it has been shown that the ODA solution exhibits some deviations with respect to the average profiles obtained from the PSS. This could suggest that the LCP can not accurately predict the spatial variations of K_β in the $\eta-\omega$ inter-region or that the GTE derived using the volume averaging method is not completely valid. To address these questions, in the next section, we predict the spatial variations of K_β by using the pore-scale fields arising from the PSS, and we solve the ODA again.

Table 2: Relative error percentage of the ODA, using K_β obtained from the solution of the LCP, with respect to the average of the local fields to predict the maximum velocity in the homogeneous free fluid region for several values of r_0 and two values of $\varepsilon_{\beta\omega}$.

	centered circle	
r_0/ℓ	$\varepsilon_{\beta\omega}=0.4$	$\varepsilon_{\beta\omega}=0.8$
1	4.01×10^{-2}	4.82×10^{-2}
2	7.10×10^{-2}	7.23×10^{-2}
5	1.62×10^{-1}	1.43×10^{-1}
10	3.09×10^{-1}	2.56×10^{-1}
15	4.49×10^{-1}	3.63×10^{-1}

5. ODA solution II: GTE in terms of K_β from the pore-scale solution

5.1. Prediction of K_β from the pore-scale solution

As seen in the previous section, when the spatial variations of K_β predicted from the solution of the LCP are used, the ODA solution exhibit some deviations in the $\eta-\omega$ inter-region. An alternative approach to overcome such a problem is to compute the spatial variations of K_β by using the pore-scale fields arising from the PSS. This will allow evaluating both the predictive capabilities of the LCP and the validity of the GTE derived using the volume averaging method.

To this end, by introducing Eq. (9) into Eq. (10) and using the definition given by (12), the permeability tensor can be written as

$$-\mu_\beta \varepsilon_\beta(\mathbf{x}) \mathbf{K}_\beta^{-1}(\mathbf{x}) \cdot \langle \mathbf{v}_\beta \rangle^\beta = \mathbf{f}_\beta(\mathbf{x}) \tag{21}$$

Notice that the left-hand side of the above equation results from the development of the LCP, while the right-hand side results from the averaging procedure. In this way, to predict the spatial variation of the permeability, the intrinsic average velocity and the vector $\mathbf{f}_\beta(\mathbf{x})$ should be computed using the pore-scale fields arising from the PSS. Here, for the sake of consistency, the PSS performed in the previous section was used. In addition, the shape and size of the averaging volume were chosen to be equal to those used to compute K_β from the LCP and $\langle u \rangle^\beta$ from the PSS. It is worth mentioning that a similar strategy was used by Breugem (2005), using a porous medium model which only consists of seven squares, so their system does not satisfy the disparity of characteristic length-scale given by $\ell \ll r_0 \ll L$.

In Fig. 7 we plot the spatial variations of the the $xx-$component of K_β^{-1} in the $\eta - \omega$ inter-region taking different values of r_0 for two values of $\varepsilon_{\beta\omega}$. Notice that these results are similar to those obtained from the solution of the LCP. Here K_β^{-1} also undergoes abrupt changes from its value in bulk of the porous medium (*i.e.*, at $y \leq -(r_0 + 3\ell)$) to that in the bulk of free flow region (*i.e.*, $y \geq r_0$). In addition, the value of K_β^{-1} decreases as the size of r_0 is increased, and it increases as $\varepsilon_{\beta\omega}$ is increased. On the other hand, it should be noticed that K_β^{-1} obtained from the PSS reaches the value of $K_{\beta\omega}^{-1}$ approximately at $y \approx -(3\ell + r_0)$ instead of at $y \approx -(\ell + r_0)$, as shown by predictions obtained from the solution of the LCP (see Fig. 4). This is attributed to some pore-scale information has been lost in the derivation of the LCP. Thus, the zone of changes of K_β^{-1} predicted from the PSS is restricted to the positions given by $-(3\ell + r_0) \leq y \leq +r_0$, and therefore it has a thickness equal to $2r_0 + 3\ell$, which is two unit cells larger than the size of the averaging region, as suggested in several studies (Valdés-Parada et al., 2007b, 2009b, 2013). This confirms that the zone of changes of K_β does not necessarily coincide with the one corresponding to ε_β.

5.2. Solution of the ODA in terms of K_β obtained from the PSS

Once the spatial variations of the permeability were predicted using the PSS, it is necessary to reevaluate the capabilities of the GTE to predict the average velocity profiles in the free flow/porous medium system shown in Fig. 2. To this end, in this section, we compare again the average velocity profiles obtained from the ODA solution with those from averaging the local velocity profiles resulting from the PSS. It should be recalled that the ODA is given by Eq. (15)

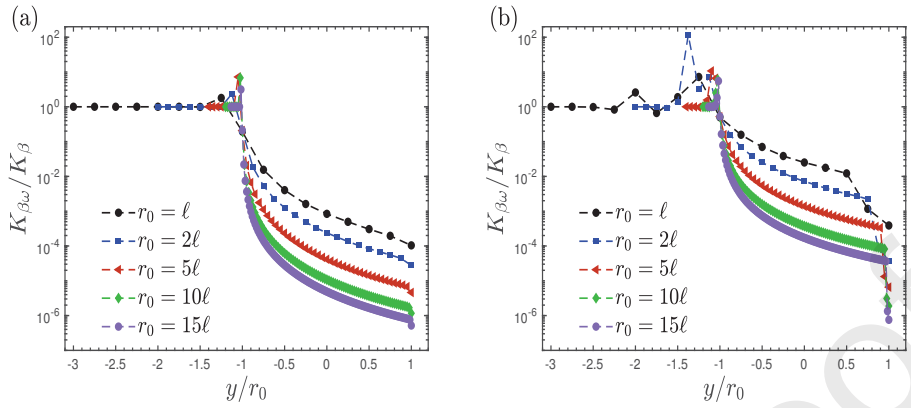

Figure 7: Spatial variations of permeabilities ratio $K_{\beta\omega}/K_\beta\,(Y)$ in the free flow/porous medium inter-region. The porous medium model consisting of a periodic array of a unit cell with a centered circle. The calculations were obtained by filtering the microscopic results using different sizes of r_0 for two values of $\varepsilon_{\beta\omega}$: (a) 0.4 and (b) 0.8.

and the boundary conditions are given by Eqs. (16). In addition, the pressure drop in both the free flow and the porous medium regions is a constant, which is given by Eq. (17). In this way, due to position dependence of the effective coefficients, the ODA was numerically solved again. It is important to remark that here the ODA is solved taking into account the spatial variations of K_β predicted using the local fields resulting from the PSS. Some examples of the intrinsic average velocity profiles are shown below according to Eq. (18).

In Fig. 8 the average velocity profiles obtained from the solution of the ODA, using the permeability predicted from the PSS, and the average of the local velocity fields are compared. These profiles are for different values of r_0 and $\varepsilon_{\beta\omega} = 0.4$. The average velocity profiles in the whole domain of the channel are displayed in Fig. 8(a). From this result, it is interesting to note that the predictions of the ODA improve significantly when the predictions of the permeability obtained from the PSS are used. This is confirmed in the amplification of the maximum velocity neighborhood shown in Fig. 8(b) and especially by observing the velocity profiles in the $\eta - \omega$ inter-region shown in Fig. 8(c).

To have a more quantitative insight about the predictive capabilities of the GTE, the relative error percentage of the ODA solution with respect to the average of the PSS was computed. To this end, we evaluated the Eq. (19) and the result are shown in Table 3, as a function of r_0 for two values of $\varepsilon_{\beta\omega}$. As one can see, the error percentage in all cases is below 4 %. In addition, notice that the error percentages obtained for $\varepsilon_{\beta\omega} = 0.4$ are larger than those obtained for $\varepsilon_{\beta\omega} = 0.8$.

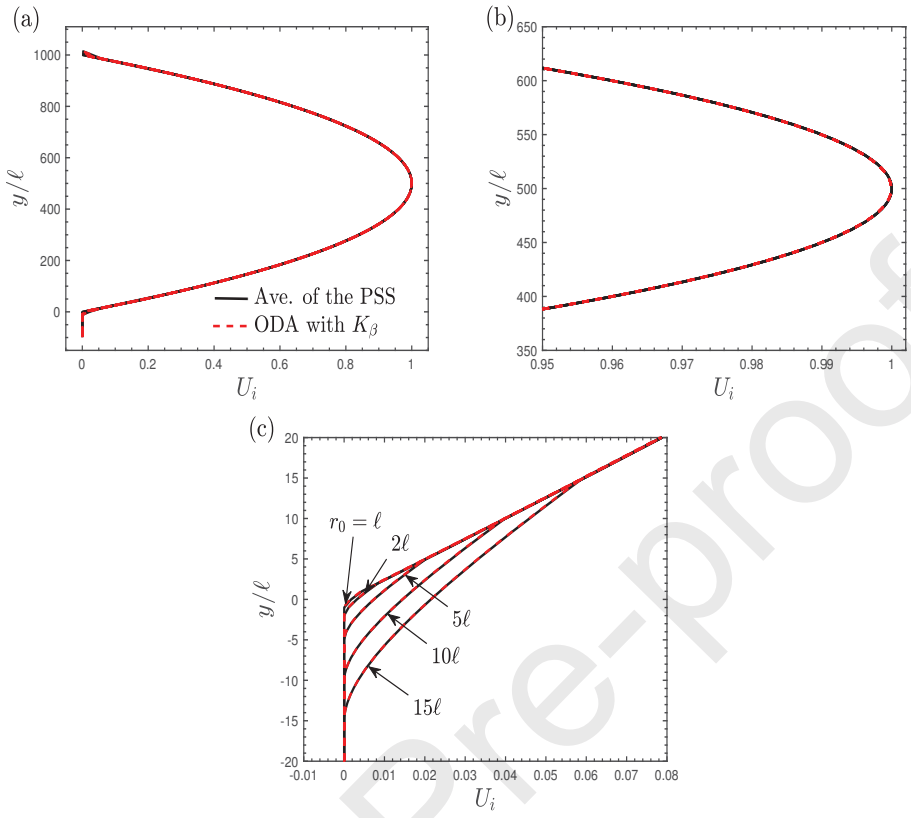

Figure 8: Comparison of the intrinsic average velocity profiles in the channel partially filled with a porous medium obtained from averaging the PSS and the ODA solution (with K_β obtained from the PSS) taking several values of r_0 for $\varepsilon_{\beta\omega} = 0.4$. The velocity profiles are (a) in the whole channel, (b) around the maximum velocity and (c) in $\eta - \omega$ inter-region. The porous medium model consist of a periodic array of a unit cells with a centered circle. In all the calculation we used $L_\eta = 10^3\ell$ and $L_\omega = 10^2\ell$.

As mentioned above, this is because when porosity increases, flow resistances decrease, and therefore the error in permeability predictions decreases. This error can be reduced if a larger number of points to sample the permeability are used. In our calculations, the distance between sampling points was $\ell/4$. We have evidence that by increasing the number of sampling points, the error percentage tends to zero.

As before, we also used Eq. (20), to compute the relative error percentage of the ODA solution with respect to the average of the PSS to predict the maximum velocity in the free flow region. These results are shown in Table 4 for different values of r_0 and two values of $\varepsilon_{\beta\omega}$. There, we can appreciate that all the relative error percentages are smaller than 10^{-2}, which confirms

Table 3: Relative error percentage of the ODA, with K_β predicted from filtering the PSS, with respect to the average of the PSS to predict the average velocity profiles in the free flow/porous medium inter-region for several values of r_0 and two-values of $\varepsilon_{\beta\omega}$.

	centered circle	
r_0/ℓ	$\varepsilon_{\beta\omega} = 0.4$	$\varepsilon_{\beta\omega} = 0.8$
1	3.36	1.87
2	3.00	1.22
5	1.16	0.47
10	0.57	0.26
15	0.36	0.17

that the errors in the predictions in the $\eta - \omega$ inter-region do not have significant effects on the predictions of the velocity profiles in the homogeneous $\eta-$region. As in the previous section, on the LCP, these observations are attributed to the dimensions of the free fluid/porous medium system satisfies a separation of characteristic length scales.

Thus, one can conclude that the GTE for total mass and momentum transport derived by using the volume averaging method can accurately predict the average velocity profiles everywhere in a free fluid/porous medium system (in the homogeneous regions and as well as in the $\eta - \omega$ inter-region) as long as the spatial variations of permeability are accurate. Therefore, the errors in the ODA solution shown in Section 4 are due to the fact that the LCP can only predict approximate spatial variations of K_β in the $\eta - \omega$ inter-region. It is worth mentioning that all these observations are also valid for $0.25 \leq \varepsilon_{\beta\omega} \leq 0.95$. In addition, we also performed the calculations using a porous medium made of a two-dimensional unit cell with a staggered arrangement of circles for $0.25 \leq \varepsilon_{\beta\omega} \leq 0.95$ and a centered square for $0.05 \leq \varepsilon_{\beta\omega} \leq 0.95$. In both cases, similar results as those for the unit cell with a centered circle were obtained. However, those results are not presented here to preserve the brevity of this work.

In the following section, we analyze the effects of the viscous terms involved in the macroscopic momentum equation, which are results of the averaging method used to derive it at the macroscale, on the average velocity profiles.

5.3. Contribution of the first and second Brinkman corrections

As seen earlier, the GTE for momentum transport includes both a first and a second Brinkman correction. The first one describes one part of the macroscopic viscous forces due to the fluid, while the second one describes another part of the macroscopic viscous forces but

Table 4: Relative error percentage of the ODA, with K_β predicted from filtering the PSS, with respect to the average of the PSS to predict the maximum average velocity in the homogeneous free fluid region for several values of r_0 and two-values of $\varepsilon_{\beta\omega}$.

	centered circle	
r_0/ℓ	$\varepsilon_{\beta\omega} = 0.4$	$\varepsilon_{\beta\omega} = 0.8$
1	7.91×10^{-3}	1.17×10^{-2}
2	7.74×10^{-3}	6.24×10^{-4}
5	7.59×10^{-3}	1.19×10^{-3}
10	7.37×10^{-3}	2.3×10^{-5}
15	7.18×10^{-3}	3.18×10^{-4}

due to the spatial variations of the porosity in the inter-regions. Notice that when the porous is homogeneous, the second Brinkman correction exists only in the inter-regions (Whitaker, 1999). However, several works suggest that the second Brinkman correction can be neglected in the inter-regions since its contributions are taken into account through the spatial variations of the porosity and the permeability tensor (Chandesris & Jamet, 2006, 2007), although it has not been demonstrated so far. In order to address this problem, in this section, the contribution of each viscous term of the GTE on the prediction of the average velocity profiles are evaluated. To this end, we solve the ODA twice, first considering the second Brinkman correction in the inter-region but not the first, and then in the other way around.

In this way, for the system under consideration, in Fig. 9 we compare the average velocity profiles obtained from the ODA solution, under the two conditions mentioned above, with those from the solution of the complete ODA and averaging the local velocity profiles resulting from the PSS. These results were obtained using the porous medium model made of a periodic array of a unit cell with a centered circle using $r_0 = 15\ell$ and $\varepsilon_{\beta\omega} = 0.4$. In the ODA solution the spatial variations of K_β predicted from filtering the PSS were used. Regarding these results, the following comments are in order

- On the one hand, by neglecting the first Brinkman correction (FBC), the ODA solution exhibits significant deviations from the average profiles obtained from the complete ODA and the PSS. These deviations can be appreciated even without making amplifications in the areas of interest (*i.e.*, in the inter-region and around the maximum velocity). Note that the ODA without the FBC underestimates the average velocity profiles presenting an abrupt change around $y = 15\ell$. This highlights the relevance of including the FBC in

Table 5: Relative error percentage of the ODA by neglecting the first and the second Brinkman corrections in the inter-region with respect to the average of the PSS to predict the average velocity profiles in the free fluid/porous medium inter-region for several values of r_0 and two values of $\varepsilon_{\beta\omega}$.

	$\varepsilon_{\beta\omega} = 0.4$		$\varepsilon_{\beta\omega} = 0.8$	
r_0/ℓ	without FBC	without SBC	without FBC	without SBC
1	99.75	32.13	99.64	2.85
2	99.50	36.07	99.26	11.09
5	98.72	38.13	98.22	10.83
10	97.44	38.36	96.48	10.73
15	96.20	38.14	94.76	10.70

the inter-region to predict the velocity profiles near porous media boundaries.

- On the other hand, by neglecting the second Brinkman correction (SBC), deviations in the prediction of the average velocity profiles are also introduced. However, these deviations are lower than those obtained by neglecting the FBC, so the average velocity profiles from the ODA without the SBC are closer to those obtained from the complete ODA and the PSS. It should be noticed that the magnitude of the introduced errors decreases everywhere in the system as the value of $\varepsilon_{\beta\omega}$ is increased.

In order to have a more quantitative insight about the introduced errors in the prediction of the average velocity profiles by neglecting the first and then the second Brinkman correction with respect to the average of the local fields, we computed the relative percentage error of each case using a similar equation to Eq. (19). In Table 5 we show the values of Error% for different values of r_0 and two values of $\varepsilon_{\beta\omega}$. From these results, we observe that the introduced errors by neglecting the FBR are larger than 95 % for all cases here considered, while by neglecting the SBC, they are larger than 10 %. Notice that these errors increase as the $\varepsilon_{\beta\omega}$ value decreases.

Finally, in order to appreciate the contribution of each term involved in the GTE for momentum transport, in Fig. 10 we plot the spatial variations of both Brinkman corrections and the friction term in the $\eta - \omega$ inter-region taking $r_0 = 15\ell$ for two values of $\varepsilon_{\beta\omega}$. As one can see, for both values of $\varepsilon_{\beta\omega}$, the FBC is of the same order of magnitude as the Darcy term. However, due to their spatial variations are of the opposite sign, their contributions tend to cancel. On the other hand, although the SBC has an order of magnitude lower than the other viscous terms, its contribution may be crucial because the other terms tend to cancel each other. It should be noted that the magnitude of all terms decreases as the value of $\varepsilon_{\beta\omega}$ increases, which indicates

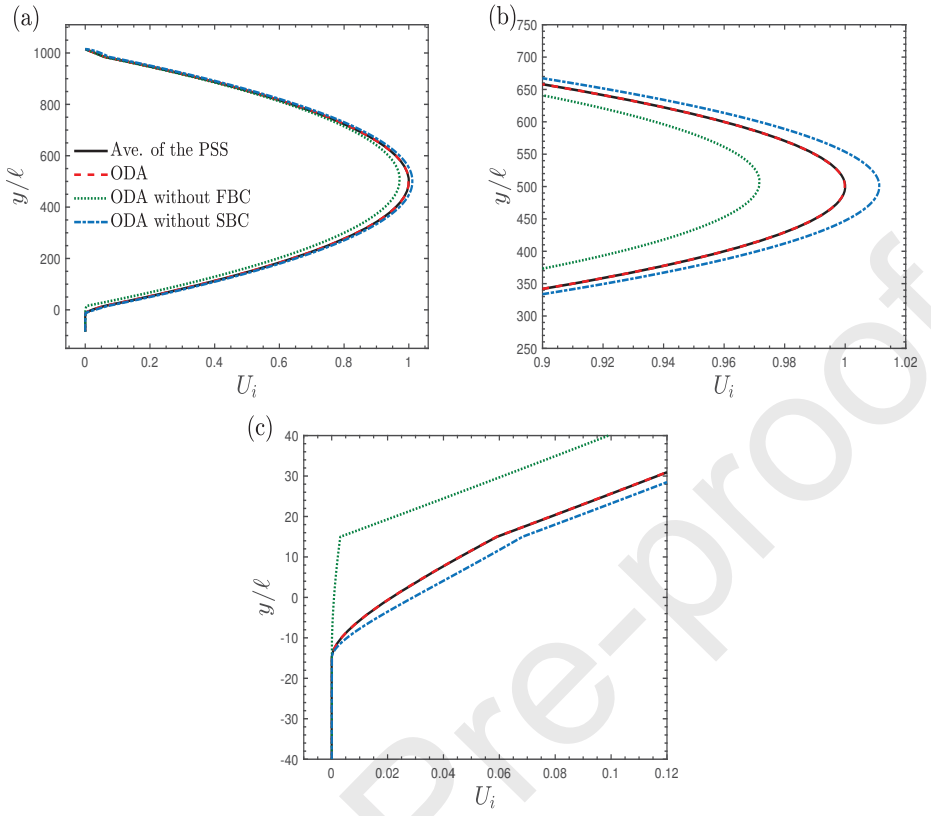

Figure 9: Comparison of intrinsic average velocity profiles in the channel partially filled a with a porous medium obtained from averaging the PSS and the ODA solution (with K_β predicted from the PSS) by neglecting the FBC and then the SBC for $r_0 = 15\ell$ and $\varepsilon_{\beta\omega} = 0.4$. The velocity profiles are (a) in the whole channel, (b) around the maximum velocity and (c) in $\eta - \omega$ inter-region. The porous medium model consist of a periodic array of a unit cell with a centered circle. The size of the free flow/porous medium system consist of $L_\eta = 10^3\ell$ and $L_\omega = 10^2\ell$.

that the flow resistances are decreased when more fluid is considered in the unit cells.

From the above, it can be concluded that to accurately predict the average velocity profiles between a free flow and a porous medium without a doubt, the first and the second Brinkman corrections in the momentum equation must be included in the $\eta - \omega$ inter-region. In addition, it is clear that the contributions of the second Brinkman correction are not necessarily taken into account through the spatial variations of the porosity and the permeability, as suggested several authors. These results confirm those outlined by Ochoa-Tapia et al. (2017); Hernandez-Rodriguez et al. (2020).

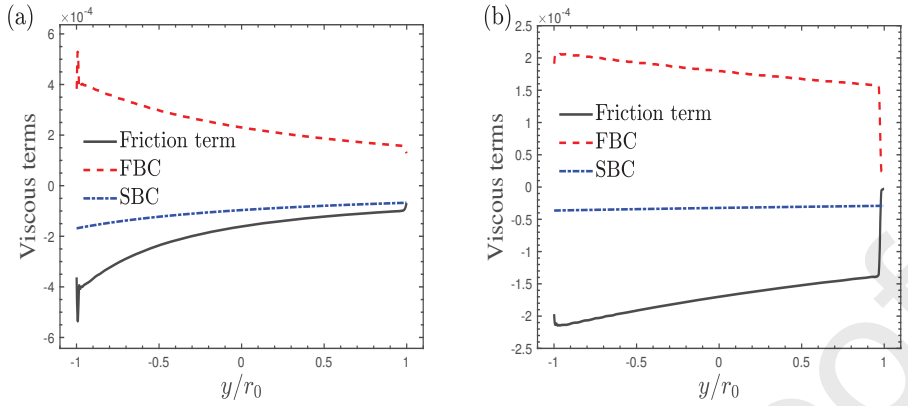

Figure 10: Spatial variations of the viscous terms in the GTE for momentum transport in the free flow/porous medium inter-region using the porous medium made of unit cells with a centered circle, $r_0 = 15\ell$ and two two values of $\varepsilon_{\beta\omega}$: (a) 0.4 and (b) 0.8. The size of the free fluid/porous medium system consist of $L_\eta = 10^3\ell$ and $L_\omega = 10^2\ell$.

6. Effect of a porous medium boundary with decreasing particle diameter

So far, the predictions of the spatial variations of the effective medium coefficients in the inter-region have been constrained to systems where, at the level of a unit cell, the porous medium is homogeneous up to its adjacent surface to the free flow region. However, in many systems, the porous medium may contain a variable particle size near its boundaries, and as a consequence, it may have different spatial variations of the effective coefficients and therefore different velocity profiles, such as in solidification processes (Goyeau et al., 1997, 1999; Bousquet-Melou et al., 2002; Roux et al., 2006; Kumar et al., 2013). In fact, in several free fluid/porous medium systems, the surface of the porous medium also presents protuberances or roughness that can modify the spatial variation of the effective coefficients and consequently the flow in the open gap, as shown by Valdés-Parada et al. (2009a). In this way, in order to analyze the effects that may have a variable particle size near the porous medium boundaries, in this section, we predict the spatial variations of the porosity and permeability in the free fluid/porous medium inter-region using a porous medium such as the one shown in Fig. 11.

The spatial variations of the effective medium coefficients were obtained by performing a PSS in a periodic representative domain of the whole channel, as described in previous sections. As shown in Fig. 11, the porous medium also consists of a periodic array of a unit cell with a centered circle. However, here the particle size in the bulk of the porous medium is constant, and it varies in a distance L_s below the surface of the porous medium. In this zone the volume

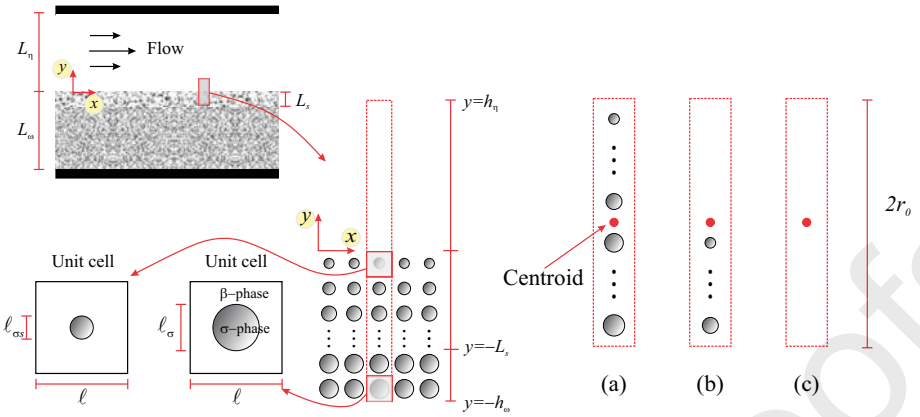

Figure 11: Sketch of the free flow/porous medium system with variable particle size near the porous medium boundaries and samples at (a) $y = -r_0$, (b) $y = 0$, and $y = +r_0$. The porous medium consist of an array of a unit cell with a centered circle.

fraction of each unit cell $\varepsilon_{\beta s}$, which is a function of the vertical position, is expressed as

$$\varepsilon_{\beta s} = \left(\frac{\varepsilon_{\beta\,\max} - \varepsilon_{\beta\,\min}}{h_\eta - \ell}\right)\left(y + h_\eta - \frac{\ell}{2}\right) + \varepsilon_{\min}, \quad \text{for } -L_s + \ell/2 \leq y \leq -\ell/2 \tag{22}$$

while the radius of the particles is given by

$$\frac{r_s}{\ell} = \left[\frac{1 - \varepsilon_{\beta s}}{\pi}\right]^{0.5} \tag{23}$$

In this way, taking different values of r_0 for $\varepsilon_{\beta\,\min} = \varepsilon_{\beta\omega} = 0.4$, $\varepsilon_{\beta\,\max} = 0.95$, the spatial variations of the effective medium coefficients were computed. On the one hand, in Fig. 12 (a) we plot the spatial variations of the fluid volume fraction in the $\eta - \omega$ inter-region. As one can observe, fluid volume fraction changes sigmoidally from its value in the bulk of the porous medium to that in the bulk of the free flow region. The zone of changes of this coefficient is restricted to the positions given by $-r_0 - L_s \leq y \leq +r_0$. On the other hand, the spatial variations of the permeability in the inter-region are shown in Fig. 12(b). In this case, one can appreciate that the spatial variations of K_β exhibits two rates of change, the first one is due to the changes in particle size, and the second one due to the averaging volume moves from a position completely located in the porous medium to that completely located in the free flow. The zone of changes of K_β is restricted to the positions given by $-(3\ell + L_s + r_0) \leq y \leq +r_0$. In this way, the zones of change of the volume fraction and permeability, when the porous medium contains a variable particle size near its boundaries, are larger than that when the porous medium is homogeneous up to its boundaries.

Finally, in Fig. 13 (a) we compare the average velocity profiles arising from the ODA solution

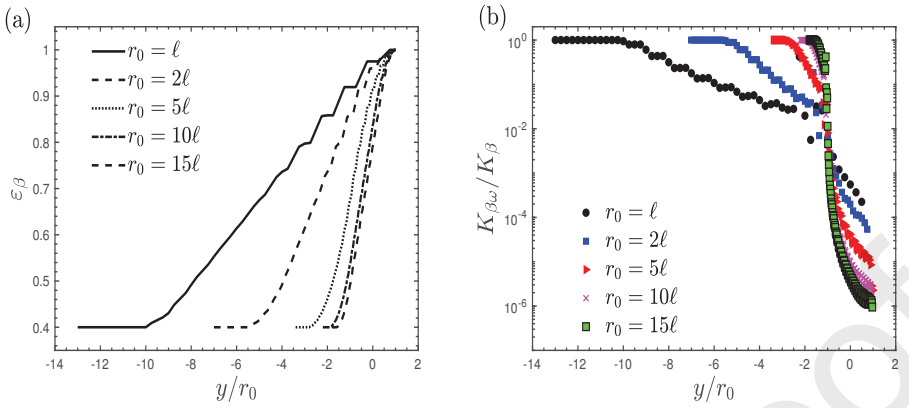

Figure 12: Spatial variations of (a) the volume fraction and (b) the permeabilities ratio $K_{\beta\omega}/K_\beta(Y)$. The porous medium consist of a periodic array of a unit cell with a centered circle which exhibit a variable particle size near the its boundaries. The prediction are obtained from filtering the pore-scale profiles taking different values of r_0 for $\varepsilon_{\beta\omega} = 0.4$ and $\varepsilon_{max} = 0.95$. In all the calculations the whole system consist of $L_\eta = 10^3\ell$, $L_\omega = 10^2\ell$ and $L_s = 10\ell$.

with those from averaging the pore-scale fields for different sizes of r_0. Due to the differences are negligible in the homogeneous regions, the comparisons are only shown in the $\eta-\omega$ inter-region. As one can observe, the ODA predictions are in good agreement with the reference profiles for all values of r_0. These results can be qualitatively confirmed in Fig. 13(b), where the same profiles are presented on a logarithmic scale. Moreover, to analyze the contribution of the viscous terms of the GTE, in Fig. 13 (c) we plot the ODA predictions when the SBC is neglected. These profiles are also shown on a logarithmic scale in Fig. 13 (d). Notice that not including the SBC in the GTE again introduces deviations in the ODA predictions. However, these deviations are larger when the particle size is variable than those obtained when the particle size is constant (see Fig. 9).

7. Discussion

Based on the above, we can make the following observations

- On the one hand, by comparing the average velocity profiles obatined from the solution of the ODA with those from averaging the local fields, it has been shown that the ODA can be suitable alternative to predict the fully developed flow in a free fluid/porous medium system, like the one studied by Beavers & Joseph (1967). To this end, the GTE for momentum transport must include two viscous terms (*i.e.*, the first and the second Brinkman

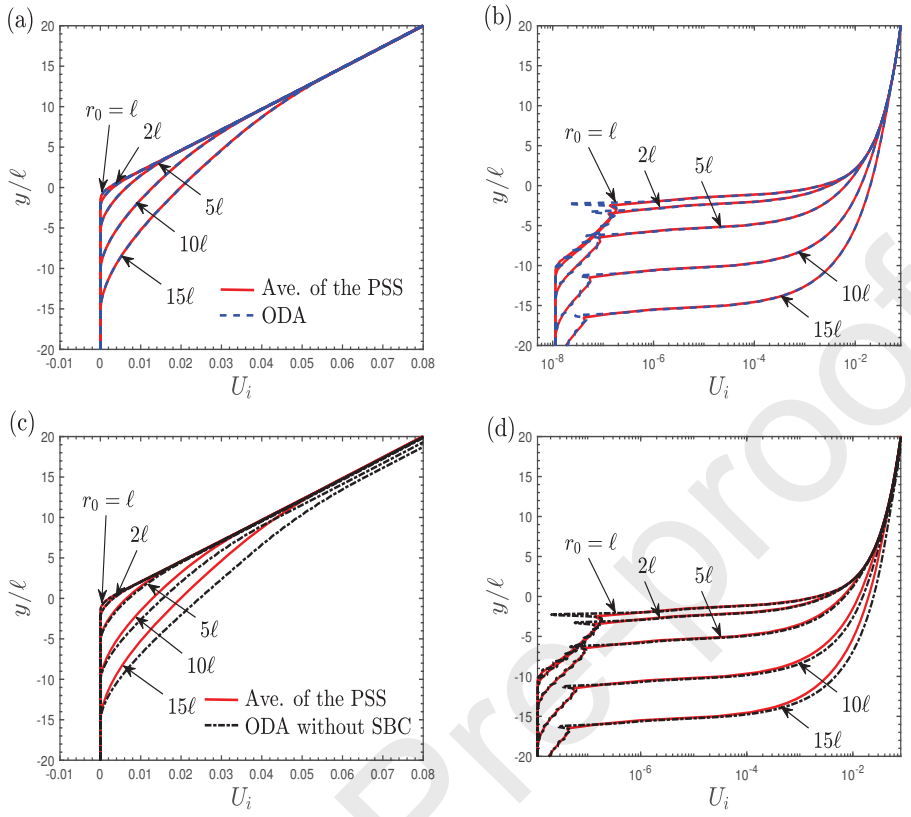

Figure 13: Comparison of the intrinsic average velocity profiles in the free flow/porous medium inter-region obtained from solving the ODA and averaging the PSS taking different values of r_0 for $\varepsilon_{\beta\omega} = 0.4$ and $\varepsilon_{max} = 0.95$. The porous medium model consist of a periodic array of a unit cell with a centered circle presenting a variable particle size in the porous medium boundary. The results in (a) an (b) are using the complete GTE and those in (c) and (d) are using GTE without the SBC. In all the calculations $L_\eta = 10^3\ell$, $L_\omega = 100\ell$ and $L_s = 10\ell$.

corrections) and a Darcy's term with a position-dependent intrinsic permeability tensor. In this way, the additional terms arising from the up-scaling method used to derive the governing equations at the macroscale can certainly be justified. It is worth stressing that including or not the additional terms in the macroscopic momentum equations could change the description of other transport quantities as heat or mass transport in a free fluid/porous medium system. In our opinion, this contributes to clarifying the range of validity of the Brinkman correction to Darcy's law that has been the subject of great debate in the literature (Vafai & Kim, 1990; Nield, 1991; Sahraoui & Kaviany, 1992; Auriault, 2009; Zampogna & Bottaro, 2016). The Brinkman corrections must be included in the inter-regions, and they can be neglected with respect to Darcy's term in the bulk of the porous

medium, as has been previously indicated by many authors (Whitaker, 1999). In addition, the effective viscosity of a porous medium must be given by $\mu_{eff} = \varepsilon_{\beta}^{-1}(\mathbf{x})\,\mu_{\beta}$. All these results were obtained for different values of r_0 (ℓ, 2ℓ, 5ℓ, 10ℓ, 15ℓ) and using a porous medium made of a periodic array of a unit cell with a centered circle ($0.25 \leq \varepsilon_{\beta\omega} \leq 0.95$) but also with a staggered arrangement of circles ($0.25 \leq \varepsilon_{\beta\omega} \leq 0.95$) and a centered square ($0.05 \leq \varepsilon_{\beta\omega} \leq 0.95$). For the sake of conciseness, the results for the last two unit cells are not presented here.

- In Fig. 14 we plot the spatial variations of K_{β} in the free flow/porous medium inter-region predicted from the solution of the LCP and those resulting from the PSS using two values of r_0 for two values of $\varepsilon_{\beta\omega}$. From this comparison, some differences can be observed between both predictions, indicating that the LCP is just an approximate alternative to predict the spatial variations of K_{β} in the inter-region. However, as it is shown in the same figure, the LCP provides better predictions of K_{β} than the empirical functions widely used in literature. For instance, an extension of the Carman-Kozeny equation, a step-jump function, and a linear function (Ochoa-Tapia & Whitaker, 1995b; Angot, 1999; Goyeau et al., 2003; Chandesris & Jamet, 2006, 2007; Chen & Wang, 2014). In addition, when these empirical predictions of K_{β} are used for solving the ODA, the resulting average velocity profiles are further away from the averages of the local profiles than those obtained when K_{β} predicted from the solution of the LCP is used. For the sake of conciseness, these average velocity profiles are not shown in this work. Therefore, until better alternatives are found to predict the spatial variations of the permeability in the inter-region, the LCP will be the best alternative available for it.

- It has been shown that the permeability variations in the free flow/porous medium inter-region depend on the size of the sampling region. This is shown by the results obtained from the LCP, Fig. 4, but also by those obtained from the PSS, Fig. 7. In addition, by using larger values of r_0, we have also found that the permeability variations in the free fluid/porous medium inter-region do not present an asymptotic behavior with respect to the size of the averaging sample. This result can be attributed to the fact that when the value of r_0 is increased more fluid is included in the averaging sample. However, it should be recalled that r_0 must be constrained by the inequality given by $r_0 \ll L_{\eta}$ in order to provide appropriate permeability and velocity predictions. Analogous observations can be also made on the average velocity profiles in the same inter-region. This was shown by

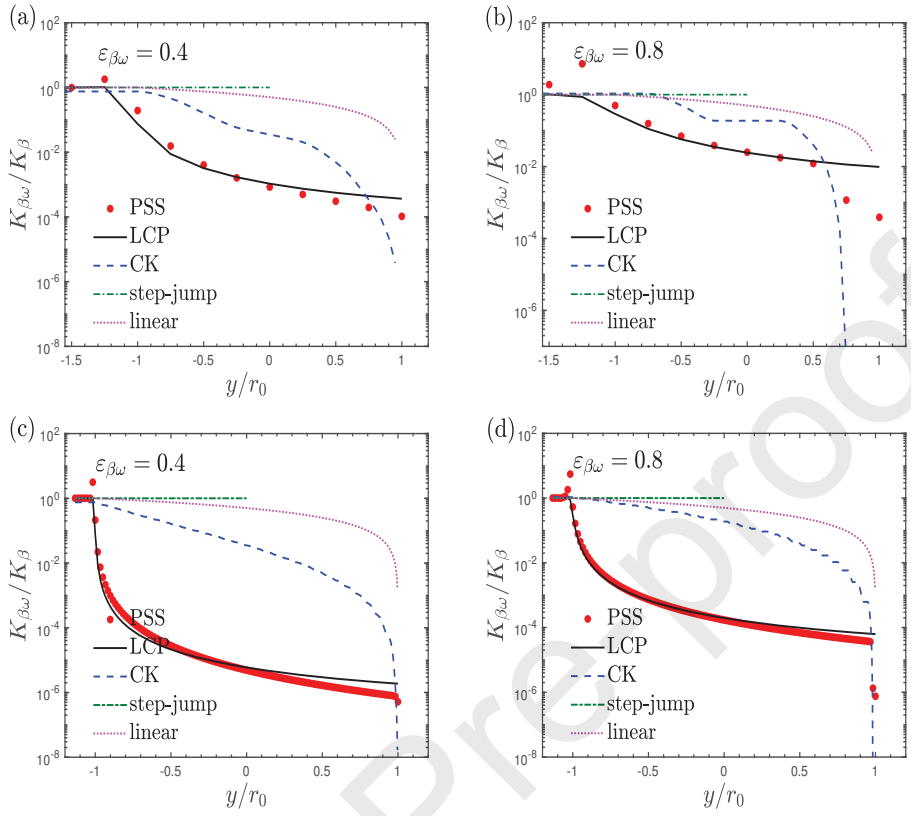

Figure 14: Comparison of the spatial variations of permeabilities ratio $K_{\beta\omega}/K_{\beta}(Y)$ in the free flow/porous medium inter-region predicted from the PSS with those predicted from the LCP, an extension of CK equation, a step-jump function and a linear function. The calculations are taking (a) $\varepsilon_{\beta\omega} = 0.4$ and $r_0 = \ell$, (b) $\varepsilon_{\beta\omega} = 0.8$ and $r_0 = \ell$, (c) $\varepsilon_{\beta\omega} = 0.4$ and $r_0 = 15\ell$, and (d) $\varepsilon_{\beta\omega} = 0.8$ and $r_0 = 15\ell$.

our research group in Ochoa-Tapia et al. (2017); Hernandez-Rodriguez et al. (2020). In fact, the dependency of the average profiles on the size and shape of the samples must be considered if the predictions are used for comparing with experimental data (Baveye & Sposito, 1984; Cushman, 1984).

- According to Valdés-Parada et al. (2009b), the height of the solution domain for the LCP must be $h_\eta + h_\omega = 40\ell$, where was assumed that $h_\eta = h_\omega$. These led them to obtain a zone of changes of permeability of thickness equal to $2r_0 = 20\ell$. However, from the PSS, we have found that the height of the solution domain for the LCP depends on the size of the averaging volume. The height h_η must be at least $2r_0$, while the height h_ω must be at least $2r_0 + 3\ell$ in all cases. Notice that the porous medium region contained in the solution domain is slightly larger than that of the free fluid region (*i.e.*, $h_\eta < h_\omega$). This

is in order to reach the value of the permeability of the bulk of the porous medium. As a consequence, the thickness of the zone of changes of permeability is equal to $2r_0 + 3\ell$.

- The results in Section 4 and those presented in Section 5 show a smooth transition zone in the average velocity profiles in the $\eta - \omega$ inter-region, from the velocity when the averaging volume is completely located in the bulk of the porous medium (*i.e.*, the Darcy velocity) to that when it is completely located in the free flow region (*i.e.*, $y = +r_0$). It is worth stressing that such a transition zone is a result of using average quantities instead of the form of the macroscopic equations resulting from up-scaling the pore-scale problem, although it can certainly be predicted from the solution of the ODA. It should be noticed that the portion of the average velocity below the surface of the porous medium (*i.e.*, $-(3\ell + r_0) \leq y \leq 0$) is what is known as the Brinkman boundary layer (Goharzadeh et al., 2005; Morad & Khalili, 2009). Recently, we have shown that the thickness of the Brinkman boundary layer depends on the size of the averaging volume, and it is approximately of the order of $\delta_B = 3\ell + r_0$ (Hernandez-Rodriguez et al., 2020). Therefore, it could be much larger than $\sqrt{K_{\beta\omega}}$, as suggested in several studies (Goyeau et al., 2003; Chandesris & Jamet, 2006, 2007; Chen & Wang, 2014).

- Finally, as mentioned earlier, an alternative approach to an ODA is a TDA, where it is necessary to develop two jump boundary conditions, one for the velocity and one for the stress. In the context of the volume averaging, these jump boundary conditions are written in terms of jump coefficients that depend on the spatial variations of the effective medium coefficients in the inter-regions (Valdés-Parada et al., 2007a, 2009a, 2013). However, prediction the effective medium coefficients have been based on the solution of the LCP, which can lead to obtain approximate effective medium coefficients, according to the results found in this work, and therefore approximate jump coefficients. In this way, the effective medium coefficients predicted from the PSS provide the opportunity to accurately predict the jump coefficients and evaluate the performance of a TDA. This and further ideas will be explored in future works. It is worth mentioning that others approaches can also be used to derive jump boundary conditions, such as the multiscale homogenization technique (Zampogna & Bottaro, 2016; Lācis & Bagheri, 2017; Bottaro & Naqvi, 2020; Sudhakar et al., 2021). In that alternative, the jump coefficients also depend on the microstructure of the porous medium near the free flow/porous medium boundary, although they do not require knowing the spatial variations of the effective medium coefficients. In

addition, all the jump coefficients can be computed by solving a set of Stokes problems in reduced computational domains.

8. Conclusions

In this work, we applied a one-domain approach to study the momentum transport between a free flow and a porous medium regions in a similar system to the one studied by Beavers & Joseph (1967). Such a model is based on closed generalized transport equations derived from the microscopic problem by applying the volume averaging method (Whitaker, 1999). In specific, for momentum transport, the resulting equation involves two viscous terms (*i.e.*, the first and the second Brinkman corrections) and a Darcy's term. In addition, it is expressed in terms of position-dependent effective medium coefficients such as the volume fraction and the intrinsic permeability tensor. Using a system where the porous medium is made of a periodic array of a two-dimensional unit cell with solid particles (*i.e.*, centered circle, staggered circles, and centered square), the first coefficient was predicted by the single integration of the $\beta-$phase within an averaging volume, and the second one from both the solution of the associated local closure problem and the pore-scale fields arising from performing pore-scale simulations.

From the above, we addressed the question about the validity of the two Brinkman's corrections and the Darcy's term expressed in terms of a position-dependent permeability tensor and if whether or not these three terms are just results of the up-scaling method used to derive the governing equations at the macroscale. To this end, we compared the average velocity profiles resulting from the solution of the one-domain approach with those arising from averaging the pore-scale fields obtained by performing pore-scale simulations. From these results, it was interesting to find out that the ODA satisfactorily reproduces the average velocity profiles obtained from the pore-scale simulations, as long as the spatial variations of the effective medium coefficients in the inter-region are exact. Therefore, the three terms involved in the generalized transport equations for momentum transport can certainly be justified. These results stand for any size of the averaging volume (r_0) and porosity value of the bulk of the porous medium ($\varepsilon_{\beta\omega}$).

Regarding the two approaches used to predict the permeability in the inter-region different average velocity profiles from the solution of the macroscopic model were obtained. On the one hand, when the spatial variations of the permeability are obtained from the solution of the local closure problem, it has been found out that the resulting profiles from the solution of the macroscopic model exhibit some deviations in the inter-region with respect to the average of the local fields. This is attributed to the fact that the local closure problem is only an approximate

approach to predict the permeability in the inter-region. However, we have found that it provides better predictions of the permeability than the empirical expressions commonly used in the literature (*i.e.*, linear, step-jump or hyperbolic function, etc.). On the other hand, when the spatial variations of the permeability are obtained from filtering pore-scale profiles, the average velocity profiles from the solution of the macroscopic model are in excellent agreement with the averages of the pore-scale fields.

Analyzing the two Brinkman's corrections, we have found that both viscous terms are crucial for predicting the average velocity profiles everywhere in the free/fluid porous medium system but mainly in the inter-region. When one of these two terms is neglected in the inter-region, important deviations are introduced in the predictions, which are larger when the first Brinkman correction is neglected. From the above, we can conclude that both Brinkmans's corrections must be included in order to obtain accurate predictions of the velocity profiles.

On the other hand, we have shown that a Brinkman's boundary layer appears when the porous medium is homogeneous up to its boundaries but also when it presents a variable particle size near its boundaries. From these results, it is clear that the Brinkman's boundary layer is a result of using average quantities, although it can be reproduced by the solution of the ODA. In addition, it is interesting to notice that the size of these layers depends on the corresponding size of the averaging volume.

Finally, it should be mentioned that the results presented in this work complement those presented by Ochoa-Tapia et al. (2017); Hernandez-Rodriguez et al. (2020). Moreover, they constitute the first step on the formal derivation of exact jump boundary conditions that complete the statement of the two-domain approach for the momentum transport between a free flow and a porous medium. This is because now we already know the terms that the generalized transport equations must include since the jump boundary conditions are usually derived from the difference between the generalized transport equations and the governing equations of each homogeneous region, as shown by Valdés-Parada et al. (2013). This idea can certainly be extended to study other types of transport situations, such as the study of multiphase flows between two homogeneous regions (*e.g.*, between a free flow and a porous medium or between two porous media). These and other applications will be studied in future works.

Acknowledgments

This work was benefited from Fondo Sectorial de Investigaciıon para la educación from CONACyT (Project number: 256231). In addition, RHR (Scholarship number: 711177) ex-

presses his gratitude to CONACyT for the economical support bestowed to carry out his doctoral studies.

References

Aguilar-Madera, C. G., Valdés-Parada, F. J., Goyeau, B., & Ochoa-Tapia, J. A. (2011). Convective heat transfer in a channel partially filled with a porous medium. *International Journal of Thermal Sciences*, *50*, 1355–1368. doi:10.1016/j.ijthermalsci.2011.03.005.

Angot, P. (1999). Analysis of singular perturbations on the Brinkman problem for fictitious domain models of viscous flows. *Math. Meth. Appl. Sci.*, *22*, 1395–1412. doi:10.1002/(SICI)1099-1476(19991110)22:16.

Angot, P., Bruneau, C.-H., & Fabrie, P. (1999). A penalization method to take into account obstacles in incompressible viscous flows. *Numerische Mathematik*, *81*, 497–520.

Angot, P., Goyeau, B., & Ochoa-Tapia, J. A. (2017). Asymptotic modeling of transport phenomena at the interface between a fluid and a porous layer: Jump conditions. *Physical Review E*, *95*, 063302. doi:10.1103/PhysRevE.95.063302.

Auriault, J.-L. (2009). On the domain of validity of brinkmans equation. *Transport in porous media*, *79*, 215–223. doi:10.1007/s11242-008-9308-7s.

Baveye, P., & Sposito, G. (1984). The operational significance of the continuum hypothesis in the theory of water movement through soils and aquifers. *Water Resources Research*, *20*, 521–530. doi:10.1029/WR020i005p00521.

Beavers, G. S., & Joseph, D. D. (1967). Boundary conditions at a naturally permeable wall. *Journal of fluid mechanics*, *30*, 197–207. doi:10.1017/S0022112067001375.

Beavers, G. S., Sparrow, E. M., & Magnuson, R. A. (1970). Experiments on coupled parallel flows in a channel and a bounding porous medium. *Journal of Basic Engineering*, *92*, 843–848. doi:10.1115/1.3425155.

Beckermann, C., Viskanta, R., & Ramadhyani, S. (1988). Natural convection in vertical enclosures containing simultaneously fluid and porous layers. *Journal of Fluid Mechanics*, *186*, 257–284. doi:10.1017/S0022112088000138.

Bottaro, A., & Naqvi, S. B. (2020). Effective boundary conditions at a rough wall: a high-order homogenization approach. *Meccanica*, *55*, 1781–1800. doi:10.1007/s11012-020-01205-2.

Bousquet-Melou, P., Goyeau, B., Quintard, M., Fichot, F., & Gobin, D. (2002). Average momentum equation for interdendritic flow in a solidifying columnar mushy zone. *International journal of heat and mass transfer*, *45*, 3651–3665. doi:10.1016/S0017-9310(02)00077-7.

Breugem, W.-P. (2005). The influence of wall permeability on laminar and turbulent flows. In *Technische Universiteit Delft*.

Bruneau, C.-H., Creusé, E., Depeyras, D., Gilliéron, P., & Mortazavi, I. (2010). Coupling active and passive techniques to control the flow past the square back ahmed body. *Computers & Fluids*, *39*, 1875–1892. doi:10.1016/j.compfluid.2010.06.019.

Bruneau, C.-H., & Mortazavi, I. (2004). Passive control of the flow around a square cylinder using porous media. *International Journal for Numerical Methods in Fluids*, *46*, 415–433. doi:10.1002/fld.756.

Bruneau, C.-H., & Mortazavi, I. (2008). Numerical modelling and passive flow control using porous media. *Computers & Fluids*, *37*, 488–498. doi:10.1016/j.compfluid.2007.07.001.

Caltagirone, J.-P. (1994). Sur l'intéraction fluide-milieu poreux; application au calcul des efforts exercés sur un obstacle par un fluide visqueux. *Comptes rendus de l'Académie des sciences. Série II, Mécanique, physique, chimie, astronomie*, *318*, 571–577.

Carraro, T., Goll, C., Marciniak-Czochra, A., & Mikelić, A. (2015). Effective interface conditions for the forced infiltration of a viscous fluid into a porous medium using homogenization. *Computer Methods in Applied Mechanics and Engineering*, *292*, 195–220. doi:10.1016/j.cma.2014.10.050.

Chandesris, M., & Jamet, D. (2006). Boundary conditions at a planar fluid–porous interface for a poiseuille flow. *International Journal of Heat and Mass Transfer*, *49*, 2137–2150. doi:10.1016/j.ijheatmasstransfer.2005.12.010.

Chandesris, M., & Jamet, D. (2007). Boundary conditions at a fluid–porous interface: an a priori estimation of the stress jump coefficients. *International journal of heat and mass transfer*, *50*, 3422–3436. doi:10.1016/j.ijheatmasstransfer.2007.01.053.

Chandesris, M., & Jamet, D. (2009). Jump conditions and surface-excess quantities at a fluid/porous interface: a multi-scale approach. *Transport in porous media*, *78*, 419–438. doi:10.1007/s11242-008-9302-0.

Chen, H., & Wang, X.-P. (2014). A one-domain approach for modeling and simulation of free fluid over a porous medium. *Journal of Computational Physics*, *259*, 650–671. doi:10.1016/j.jcp.2013.12.008.

Cheng, P., Chowdhury, A., & Hsu, C. (1991). Forced convection in packed tubes and channels with variable porosity and thermal dispersion effects. In *Convective heat and mass transfer in porous media* (pp. 625–653). Springer. doi:10.1007/978-94-011-3220-6_20.

Cimolin, F., & Discacciati, M. (2013). Navier–stokes/forchheimer models for filtration through porous media. *Applied Numerical Mathematics*, *72*, 205–224. doi:10.1016/j.apnum.2013.07.001.

Cushman, J. H. (1984). On unifying the concepts of scale, instrumentation, and stochastics in the development of multiphase transport theory. *Water Resources Research*, *20*, 1668–1676. doi:10.1029/WR020i011p01668.

Das, S., Deen, N., & Kuipers, J. (2018). Multiscale modeling of fixed-bed reactors with porous (open-cell foam) non-spherical particles: Hydrodynamics. *Chemical Engineering Journal*, *334*, 741–759. doi:10.1016/j.cej.2017.10.047.

Eggenweiler, E., & Rybak, I. (2020). Unsuitability of the beavers–joseph interface condition for filtration problems. *Journal of Fluid Mechanics*, *892*. doi:10.1017/jfm.2020.194.

George, G. R., Bockelmann, M., Schmalhorst, L., Beton, D., Gerstle, A., Torkuhl, L., Lindermeir, A., & Wehinger, G. D. (2021). Workflow for computational fluid dynamics modeling of fixed-bed reactors packed with metal foam pellets: Hydrodynamics. *AIChE Journal*, (p. e17284). doi:10.1002/aic.17284.

Gobin, D., Goyeau, B., & Neculae, A. (2005). Convective heat and solute transfer in partially porous cavities. *International Journal of Heat and Mass Transfer*, *48*, 1898–1908. doi:10.1016/j.ijheatmasstransfer.2004.12.016.

Gobin, D., Goyeau, B., & Songbe, J.-P. (1998). Double diffusive natural convection in a composite fluid-porous layer. *J. Heat Transfer.*, *120*, 234–242. doi:10.1115/1.2830047.

Goharzadeh, A., Khalili, A., & Jørgensen, B. B. (2005). Transition layer thickness at a fluid-porous interface. *Physics of Fluids*, *17*, 057102. doi:10.1063/1.1894796.

Goyeau, B., Benihaddadene, T., Gobin, D., & Quintard, M. (1997). Averaged momentum equation for flow through a nonhomogenenous porous structure. *Transport in porous media*, *28*, 19–50. doi:10.1023/A:1006578602112.

Goyeau, B., Gobin, D., Benihaddadene, T., & Quintard, M. (1999). Numerical calculation of the permeability in a dendritic mushy zone. *Metallurgical and Materials Transactions B*, *30*, 613–622. doi:10.1007/s11663-999-0022-9.

Goyeau, B., Lhuillier, D., Gobin, D., & Velarde, M. (2003). Momentum transport at a fluid–porous interface. *International Journal of Heat and Mass Transfer*, *46*, 4071–4081. doi:10.1016/S0017-9310(03)00241-2.

Gray, W. G. (1975). A derivation of the equations for multi-phase transport. *Chemical Engineering Science*, *30*, 229–233. doi:10.1016/0009-2509(75)80010-8.

Hernandez-Rodriguez, R., Goyeau, B., Angot, P., & Ochoa-Tapia, J. (2020). Average velocity profile between a fluid layer and a porous medium: Brinkman boundary layer. *Revista Mexicana De Ingenieria Quimica*, *19*, 495–520. doi:10.24275/rmiq/Fen843.

Howes, F. A., & Whitaker, S. (1985). The spatial averaging theorem revisited. *Chemical engineering science*, *40*, 1387–1392. doi:10.1016/0009-2509(85)80078-6.

Hussong, J., Breugem, W.-P., & Westerweel, J. (2011). A continuum model for flow induced by metachronal coordination between beating cilia. *Journal of fluid mechanics*, *684*, 137.

Jäger, W., & Mikelić, A. (2009). Modeling effective interface laws for transport phenomena between an unconfined fluid and a porous medium using homogenization. *Transport in Porous Media*, *78*, 489–508. doi:10.1007/s11242-009-9354-9.

Jäger, W., Mikelic, A., & Neuss, N. (2001). Asymptotic analysis of the laminar viscous flow over a porous bed. *SIAM Journal on Scientific Computing*, *22*, 2006–2028. doi:10.1137/S1064827599360339.

Jiménez-Islas, H., Calderón-Ramírez, M., Navarrete-Bolaños, J., Botello-Álvarez, J., Martínez-González, G., & López-Isunza, F. (2009). Numerical study of natural convection in a 2-d square cavity with fluid-porous medium interface and heat generation. *Revista mexicana de ingeniería química*, *8*, 169–185.

Khalili, A., Basu, A., & Pietrzyk, U. (1998). Flow visualization in porous media via positron emission tomography. *Physics of Fluids*, *10*, 1031–1033. doi:10.1063/1.869627.

Kumar, A., Založnik, M., Combeau, H., Goyeau, B., & Gobin, D. (2013). A numerical simulation of columnar solidification: influence of inertia on channel segregation. *Modelling and Simulation in Materials Science and Engineering*, *21*, 045016. doi:10.1088/0965-0393/21/4/045016.

Lācis, U., & Bagheri, S. (2017). A framework for computing effective boundary conditions at the interface between free fluid and a porous medium. *Journal of Fluid Mechanics*, *812*, 866–889. doi:10.1017/jfm.2016.838.

Morad, M. R., & Khalili, A. (2009). Transition layer thickness in a fluid-porous medium of multi-sized spherical beads. *Experiments in Fluids*, *46*, 323. doi:10.1007/s00348-008-0562-9.

Nield, D. (1991). The limitations of the brinkman-forchheimer equation in modeling flow in a saturated porous medium and at an interface. *International Journal of Heat and Fluid Flow*, *12*, 269–272. doi:10.1016/0142-727X(91)90062-Z.

Ochoa-Tapia, J. A., Valdés-Parada, F. J., Goyeau, B., & Lasseux, D. (2017). Fluid motion in the fluid/porous medium inter-region. *Revista Mexicana de Ingeniería Química*, *16*, 923938.

Ochoa-Tapia, J. A., & Whitaker, S. (1995a). Momentum transfer at the boundary between a porous medium and a homogeneous fluid -i. theoretical development. *International Journal of Heat and Mass Transfer*, *38*, 2635–2646. doi:10.1016/0017-9310(94)00346-W.

Ochoa-Tapia, J. A., & Whitaker, S. (1995b). Momentum transfer at the boundary between a porous medium and a homogeneous fluid-ii. comparison with experiment. *International Journal of Heat and Mass Transfer*, *38*, 2647–2655.

Richardson, S. (1971). A model for the boundary condition of a porous material. part 2. *Journal of Fluid Mechanics*, *49*, 327–336. doi:10.1017/S002211207100209X.

Roux, P., Goyeau, B., Gobin, D., Fichot, F., & Quintard, M. (2006). Chemical non-equilibrium modelling of columnar solidification. *International journal of heat and mass transfer*, *49*, 4496–4510. doi:10.1016/j.ijheatmasstransfer.2006.05.020.

Rybak, I., Schwarzmeier, C., Eggenweiler, E., & Rüde, U. (2020). Validation and calibration of coupled porous-medium and free-flow problems using pore-scale resolved models. *Computational Geosciences*, (pp. 1–15). doi:10.1007/s10596-020-09994-x.

Sahraoui, M., & Kaviany, M. (1992). Slip and no-slip velocity boundary conditions at interface of porous, plain media. *International Journal of Heat and Mass Transfer*, *35*, 927–943. doi:10.1016/0017-9310(92)90258-T.

Sudhakar, Y., Lācis, U., Pasche, S., & Bagheri, S. (2021). Higher-order homogenized boundary conditions for flows over rough and porous surfaces. *Transport in Porous Media*, *136*, 1–42. doi:10.1007/s11242-020-01495-w.

Taylor, G. (1971). A model for the boundary condition of a porous material. part 1. *Journal of Fluid Mechanics*, *49*, 319–326. doi:10.1017/S0022112071002088.

Vafai, K., & Kim, S. (1990). Fluid mechanics of the interface region between a porous medium and a fluid layeran exact solution. *International Journal of Heat and Fluid Flow*, *11*, 254–256. doi:10.1016/0142-727X(90)90045-D.

Vafai, K., & Tien, C. (1982). Boundary and inertia effects on convective mass transfer in porous media. *International Journal of Heat and Mass Transfer*, *25*, 1183–1190. doi:10.1016/0017-9310(82)90212-5.

Vafai, K., & Tien, C. L. (1981). Boundary and inertia effects on flow and heat transfer in porous media. *International Journal of Heat and Mass Transfer*, *24*, 195–203. doi:10.1016/0017-9310(81)90027-2.

Valdés-Parada, F. J., Aguilar-Madera, C. G., Ochoa-Tapia, J. A., & Goyeau, B. (2013). Velocity and stress jump conditions between a porous medium and a fluid. *Advances in water resources*, *62*, 327–339. doi:10.1016/j.advwatres.2013.08.008.

Valdés-Parada, F. J., Alvarez-Ramírez, J., Goyeau, B., & Ochoa-Tapia, J. A. (2009a). Computation of jump coefficients for momentum transfer between a porous medium and a fluid using a closed generalized transfer equation. *Transport in porous media*, *78*, 439–457. doi:10.1007/s11242-009-9343-z.

Valdés-Parada, F. J., Alvarez-Ramírez, J., Goyeau, B., & Ochoa-Tapia, J. A. (2009b). Jump condition for diffusive and convective mass transfer between a porous medium and a fluid involving adsorption and chemical reaction. *Transport in porous media*, *78*, 459–476. doi:10.1007/s11242-009-9343-z.

784 Valdés-Parada, F. J., Goyeau, B., & Ochoa-Tapia, J. A. (2007a). Jump momentum boundary condition at a fluid–porous dividing surface: derivation of the closure problem. *Chemical*
786 *engineering science*, *62*, 4025–4039. doi:10.1016/j.ces.2007.04.042.

Valdés-Parada, F. J., Ochoa-Tapia, J. A., & Alvarez-Ramirez, J. (2007b). Diffusive mass trans-
788 port in the fluid–porous medium inter-region: Closure problem solution for the one-domain approach. *Chemical Engineering Science*, *62*, 6054–6068. doi:10.1016/j.ces.2007.06.012.

790 Whitaker, S. (1999). *The method of volume averaging*. Kluwer Academic Publishers.

Zampogna, G. A., & Bottaro, A. (2016). Fluid flow over and through a regular bundle of rigid
792 fibres. *Journal of Fluid Mechanics*, *792*, 5–35. doi:10.1017/jfm.2016.66.

Nomenclature

$\mathscr{A}_{\beta\sigma}$	interfacial domain between the solid and fluid phases within the averaging volume
$\mathscr{A}_{\beta\sigma,M}$	interfacial domain between the solid and fluid phase in the entire fluid-porous medium system
$\mathscr{A}_{\beta e,M}$	interfacial domain at the entrances or exits of the $\beta-$phase in the entire fluid-porous medium system
$\mathbf{b}_\beta$	closure variable that maps $\mu_\beta\langle\mathbf{v}_\beta\rangle^\beta$ onto $\tilde{p}_\beta$, m^{-1}
$\mathbf{B}_\beta$	closure variable that maps $\langle\mathbf{v}_\beta\rangle^\beta$ onto $\tilde{\mathbf{v}}_\beta$
$\mathbf{d}_\beta$	closure variable that maps $\mu_\beta\langle\mathbf{v}_\beta\rangle^\beta$ onto $\tilde{p}_\beta$, m^{-1}
$\mathbf{D}_\beta$	closure variable that maps $\langle\mathbf{v}_\beta\rangle^\beta$ onto $\tilde{\mathbf{v}}_\beta$, m^2
C	dimensionless magnitude of the macroscopic pressure drop
$\mathbf{f}_\beta(\mathbf{x})$	non-homogeneous vector in the GTE for momentum transport, N m^{-3}
$\mathbf{g}$	gravity vector, m^2 s^{-1}
h_λ	height of the $\lambda-$region ($\lambda = \eta, \omega$) in the representative domain used for the solution of the LCP, m
$\mathbf{I}$	the identity tensor
$\mathbf{K}_\beta(\mathbf{x})$	permeability tensor valid everywhere in the system, m^2
$K_\beta(y)$	$xx-$component of the permeability tensor valid everywhere in the system, m^2
$\mathbf{K}_{\beta\omega}$	permeability tensor of the bulk of the $\omega-$region, m^2
$K_{\beta\omega}$	$xx-$component of the permeability tensor of the bulk of the $\omega-$region, m^2
L_j	characteristic length of the j-region ($j = \eta, \omega$), m
ℓ	characteristic length of the side of a unit cell that composes the $\omega-$region, m
ℓ_σ	characteristic length of the solid particle in a unit cell that composes the ω-region, m
$\mathbf{n}_{\beta\sigma}$	unit normal vector directed from the $\beta-$phase toward the $\sigma-$phase
p	dimensionless local pressure of the $\beta-$phase
p_β	local pressure of the $\beta-$phase, N m^{-2}
$\tilde{p}_\beta$	deviations of the local pressure of the $\beta-$phase, N m^{-2}
$\mathbf{r}_\beta$	position vector relative to a reference system locating the *beta*$-$phase contained in the averaging volume, m

r_0	characteristic length of the averaging volume, m
U_i	ratio of the tangential component of the dimensionless average velocity
$\mathbf{v}_\beta$	local velocity vector of the $\beta-$phase, m s^{-1}
$\tilde{\mathbf{v}}_\beta$	deviations of the local velocity vector of the $\beta-$phase, m s^{-1}
$\langle \mathbf{v}_\beta \rangle_{\omega,\infty}$	Darcy velocity vector, m s^{-1}
V	volume of the averaging domain
$\mathscr{V}$	domain of the averaging volume
$V_\beta(\mathbf{x})$	volume of the $\beta-$phase contained within the averaging domain, m^3
$\mathscr{V}_\beta(\mathbf{x})$	domain of the $\beta-$phase contained within the averaging volume
$\mathscr{V}_\sigma(\mathbf{x})$	domain of the $\sigma-$phase contained within the averaging volume
$\mathbf{x}$	position vector relative to a reference system locating the centroid of the averaging volume, m
x	horizontal coordinate, m
X	dimensionless horizontal coordinate
$\mathbf{y}_\beta$	position vector relative to the centroid locating the $\beta-$phase contained in the averaging volume, m
y	vertical coordinate, m
Y	dimensionless vertical coordinate

Greek symbols

β	fluid phase
σ	solid phase
δ_B	thickness of the Brinkman boundary layer, m
μ_β	dynamic viscosity of the $\beta-$phase, N s m^{-2}
ρ_β	density of the $\beta-$phase, kg m^{-3}
$\varepsilon_\beta(\mathbf{x})$	volume fraction of the $\beta-$phase valid everywhere in the system
$\varepsilon_{\beta\omega}$	volume fraction of the $\beta-$phase in the bulk of the $\omega-$region
ψ_β	arbitrary function associated to the $\beta-$phase
$\langle \psi_\beta \rangle$	superficial average of ψ_β
$\langle \psi_\beta \rangle^\beta$	intrinsic average of ψ_β

Abreviations

GTE	generalized transport equations
LCP	local closure problem
ODA	one-domain approach
TDA	two-domain approach

Appendix A. The local closure problem

In this section, in order to close the GTE given by Eq. (4b), we derive and formally solve the boundary-value problem for the local velocity and local pressure deviations. To this end, the governing equations for the deviations can be obtained by introducing Eq. (6) into Eqs. (1a) and (1b) and then subtracting to the result the Eqs. (4a) and (4b), respectively, to obtain

$$\nabla \cdot \tilde{\mathbf{v}}_\beta = \underbrace{(\nabla \ln \varepsilon_\beta) \cdot \langle \mathbf{v}_\beta \rangle^\beta \big|_{\mathbf{x}}}_{\text{source}} \qquad \text{in the } \beta\text{−phase} \tag{A.1a}$$

$$\begin{aligned} \mathbf{0} = -\nabla \tilde{p}_\beta + \mu_\beta \nabla^2 \tilde{\mathbf{v}}_\beta - \underbrace{\mu_\beta \varepsilon_\beta^{-1} (\nabla \varepsilon_\beta) \cdot \nabla \langle \mathbf{v}_\beta \rangle^\beta \big|_{\mathbf{x}}}_{\text{source}} \\ - \underbrace{\mu_\beta \varepsilon_\beta^{-1} \left(\nabla^2 \varepsilon_\beta\right) \langle \mathbf{v}_\beta \rangle^\beta \big|_{\mathbf{x}}}_{\text{source}} - \mathbf{f}_\beta(\mathbf{x}) \qquad \text{in the } \beta\text{−phase} \end{aligned} \tag{A.1b}$$

To achieve the above equations, in Eq. (6), it was assumed that $\langle \psi_\beta \rangle^\beta \big|_{\mathbf{r}_\beta} \approx \langle \psi_\beta \rangle^\beta \big|_{\mathbf{x}}$, which is valid when the length-scale constraints given by $r_0 \ll L$ and $r_0^2 \ll L$ are satisfied (Valdés-Parada et al., 2007a). Then, in order to complete the statement of the boundary value problem for the deviations, the corresponding boundary conditions for the local deviations can be obtained by introducing Eq. (6) into Eq. (1c), which leads to

$$\text{B. C. 1:} \quad \tilde{\mathbf{v}}_\beta = -\underbrace{\langle \mathbf{v}_\beta \rangle^\beta \big|_{\mathbf{x}}}_{\text{source}} \quad \text{at} \quad \mathscr{A}_{\beta\sigma,M} \tag{A.1c}$$

Furthermore, far enough away from the surface of the porous medium, the local deviations will correspond to those of the bulk of each region. First, in the free flow region, at a distance sufficiently above the surface of the porous medium, the local deviations will be equal to zero. Second, in the porous medium region, at a distance sufficiently below the surface of the porous medium, the local deviations will be equal to those of the bulk of the porous medium. Therefore, the solution domain for the local deviations problem can be restricted to a periodic representative domain of the free flow/porous medium boundary ($\mathscr{V}_{\eta\omega}$) large enough to contain the $\eta-\omega$ inter-region, such as the one shown in Fig. A.15. With this in mind, the following boundary conditions

for the local deviations can also be imposed

$$\text{B. C. 2:} \quad \tilde{\mathbf{v}}_\beta = \mathbf{0} \quad \text{at} \quad y = h_\eta \tag{A.1d}$$

$$\text{B. C. 3:} \quad \tilde{\mathbf{v}}_\beta = \tilde{\mathbf{v}}_{\beta\omega} \quad \text{at} \quad y = -h_\omega \tag{A.1e}$$

$$\text{Periodicity :} \quad \tilde{\mathbf{v}}_\beta(\mathbf{r}) = \tilde{\mathbf{v}}_\beta(\mathbf{r} + \mathbf{l}_i) \qquad i = x, z \tag{A.1f}$$

$$\text{Periodicity :} \quad \tilde{p}_\beta(\mathbf{r}) = \tilde{p}_\beta(\mathbf{r} + \mathbf{l}_i) \qquad i = x, z \tag{A.1g}$$

$$\text{Constraint :} \quad \langle \tilde{\mathbf{v}}_\beta \rangle^\beta = 0 \tag{A.1h}$$

$$\text{Constraint :} \quad \langle \tilde{p}_\beta \rangle^\beta = 0 \tag{A.1i}$$

where h_λ (with $\lambda = \eta, \omega$) denotes the height of the portion of the $\lambda-$region ($\mathscr{V}_\lambda$) contained in $\mathscr{V}_{\eta\omega} = \mathscr{V}_\omega + \mathscr{V}_\eta$ and $\tilde{\mathbf{v}}_{\beta\omega}$ denotes the local velocity deviations in the bulk of the porous medium. Notice that periodic boundary conditions for the local velocity and local pressure deviations are imposed in the horizontal directions (*i.e.*, in the x and z directions), which are given by Eqs. (A.1f) and (A.1g), respectively. In addition, to have a well-posed deviations problem, the local pressure deviations are bounded by an integral constraint given by Eq. (A.1i). The local velocity deviations satisfy a similar integral constraint, which is given by Eq. (A.1h), although it is unnecessary. An example of the solution domain for the local deviations problem using a periodic porous medium model is shown in Fig. 3.

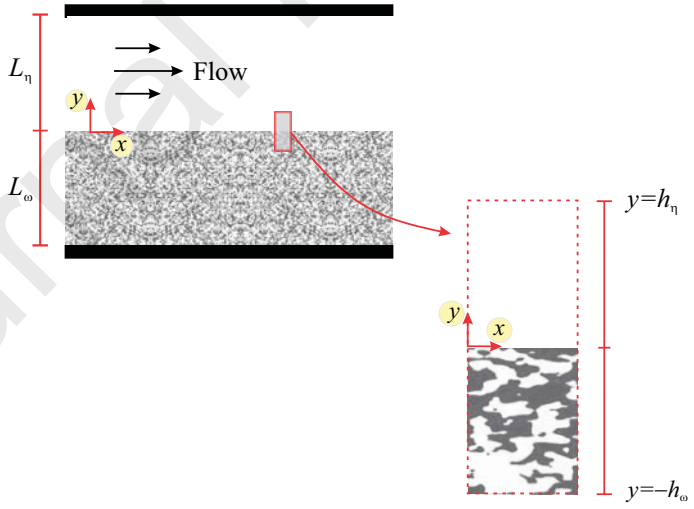

Figure A.15: Periodic representative domain of the free flow/porous medium boundary, which includes the free flow/porous medium inter-region, for the solution of the LCP.

In this way, on the basis of the length-scale constraints given by

$$\frac{r_0}{L} \ll 1; \quad \frac{r_0^2}{L^2} \ll 1; \quad \frac{\ell^2}{r_0 L} \ll 1, \tag{A.2}$$

one can use the principle of superposition to express the local deviations fields in terms of the source term given by $\langle \mathbf{v}_\beta \rangle^\beta |_{\mathbf{x}}$, as shown in Eqs. (9). To obtain this result the source term given by $\nabla \langle \mathbf{v}_\beta \rangle^\beta |_{\mathbf{x}}$ has been assumed to be negligible provided the third inequality given by Eq. (A.2) is satisfied (Valdés-Parada et al., 2007a). It should be recalled that in Eq. (9) the vector $\mathbf{b}_\beta$ and the tensor $\mathbf{B}_\beta$ are referred to as local closure variables, which maps how the constant sources are distributed into the local pressure and velocity deviations, respectively. In this way, by introducing Eqs. (9) into Eqs. (A.1), one can extract the boundary value problem for the vector $\mathbf{b}_\beta$ and the tensor $\mathbf{B}_\beta$ given by

$$\nabla \cdot \mathbf{B}_\beta = \nabla \ln \varepsilon_\beta \qquad \text{in the } \beta\text{−phase} \tag{A.3a}$$

$$\mathbf{0} = -\nabla \mathbf{b}_\beta + \nabla^2 \mathbf{B}_\beta - \varepsilon_\beta^{-1} \nabla^2 \varepsilon_\beta \mathbf{I} + \varepsilon_\beta(\mathbf{x}) \mathbf{K}_\beta^{-1}(\mathbf{x}) \qquad \text{in the } \beta\text{−phase} \tag{A.3b}$$

$$\text{B. C. 1:} \quad \mathbf{B}_\beta = -\mathbf{I} \quad \text{at} \quad \mathscr{A}_{\beta\sigma} \tag{A.3c}$$

$$\text{B. C. 2:} \quad \mathbf{B}_\beta = \mathbf{0} \quad \text{at} \quad y = h_\eta \tag{A.3d}$$

$$\text{B. C. 3:} \quad \mathbf{B}_\beta = \mathbf{B}_{\beta\omega} \quad \text{at} \quad y = -h_\omega \tag{A.3e}$$

$$\text{Periodicity :} \quad \mathbf{B}_\beta(\mathbf{r}) = \mathbf{B}_\beta(\mathbf{r} + \mathbf{l}_i) \qquad i = x, z \tag{A.3f}$$

$$\text{Periodicity :} \quad \mathbf{b}_\beta(\mathbf{r}) = \mathbf{b}_\beta(\mathbf{r} + \mathbf{l}_i) \qquad i = x, z \tag{A.3g}$$

$$\text{Constraint :} \quad \langle \mathbf{B}_\beta \rangle^\beta = \mathbf{0} \tag{A.3h}$$

$$\text{Constraint :} \quad \langle \mathbf{b}_\beta \rangle^\beta = \mathbf{0} \tag{A.3i}$$

In Eq. (A.3e), $\mathbf{B}_{\beta\omega}$ is the local closure variable in the bulk of the porous medium that can be computed by solving the corresponding local closure problem in a unit cell (Whitaker, 1999). In addition, by substituting Eqs. (9) into Eq. (10), the permeability tensor $\mathbf{K}_\beta(\mathbf{x})$ can be written in terms of the local closure variables as shown in Eq. (12). At this point, it should be noticed that the boundary-value problem given by Eq. (A.3) only depends on the porosity and the geometry of the free flow/porous medium boundary and therefore the permeability tensor in the inter-region is an intrinsic property of the porous medium boundary similar to the permeability of the bulk of the porous medium.

The LCP given by Eqs. (A.3) needs to be solved in a periodic representative domain of the free flow/porous medium boundary large enough to include the free flow/porous medium inter-region, as the one shown in Fig. A.15. To this end, the periodic representative domain of

818 the boundary with a porous medium consisting of a periodic array of a unit cell was used, as the one shown in Fig. 3. The solution domain has a height $h = h_\eta + h_\omega$ and a width ℓ.

Before moving on, it should be noticed that the LCP given by Eq. (A.3) involves an integrodifferential equation, so its solution is quite complex. To overcome this issue, it is convenient to use the following change of variables suggested by Whitaker (1999)

$$\mathbf{d}_\beta = \varepsilon_\beta^{-1}(\mathbf{x})\mathbf{b}_\beta \cdot \mathbf{K}_\beta(\mathbf{x}); \qquad \mathbf{D}_\beta = \varepsilon_\beta^{-1}(\mathbf{x})\left(\mathbf{B}_\beta + \mathbf{I}\right) \cdot \mathbf{K}_\beta(\mathbf{x}) \tag{A.4}$$

which allows us arriving to the following form of the LCP

$$\nabla \cdot \mathbf{D}_\beta = \mathbf{0} \qquad \text{in the } \beta-\text{phase} \tag{A.5a}$$

$$\mathbf{0} = -\nabla \mathbf{d}_\beta + \nabla^2 \mathbf{D}_\beta + \mathbf{I} \qquad \text{in the } \beta-\text{phase} \tag{A.5b}$$

$$\text{B. C. 1:} \quad \mathbf{D}_\beta = 0 \quad \text{in} \quad \mathscr{A}_{\beta\sigma} \tag{A.5c}$$

$$\text{B. C. 2:} \quad \frac{\partial \mathbf{D}_\beta}{\partial y} = \mathbf{0} \quad \text{at} \quad y = h_\eta \tag{A.5d}$$

$$\text{B. C. 3:} \quad \frac{\partial \mathbf{D}_\beta}{\partial y} = \mathbf{0} \quad \text{at} \quad y = -h_\omega \tag{A.5e}$$

$$\text{Periodicity:} \quad \mathbf{D}_\beta\left(\mathbf{r}\right) = \mathbf{D}_\beta\left(\mathbf{r} + \mathbf{l}_i\right) \qquad i = x, z \tag{A.5f}$$

$$\text{Periodicity:} \quad \mathbf{d}_\beta\left(\mathbf{r}\right) = \mathbf{d}_\beta\left(\mathbf{r} + \mathbf{l}_i\right) \qquad i = x, z \tag{A.5g}$$

$$\text{Constraint :} \quad \langle \mathbf{d}_\beta \rangle^\beta = \mathbf{0} \tag{A.5h}$$

Notice that because in the bulk of the porous medium the closure variables fields are periodic and symmetric in the $xy-$plane, the boundary condition at $y = -h_\omega$ was replaced by a boundary condition of symmetry, which is given by Eq. (A.5e). In addition, because the permeability is infinity in the free-flow region, the field of variable $\mathbf{D}_\beta$ must be infinite there too. Therefore, the boundary condition at $y = h_\eta$ was replaced by the derivative of the variable $\mathbf{D}_\beta$ equal to zero, which is given by Eq. (A.5d). We recognize that this boundary condition at $y = h_\eta$ is more a convenience than a necessity since the solution of the original problem given by Eqs. (A.3) has not yet been obtained correctly due to its complexity. Finally, from the integral constraint that the intrinsic average of $\mathbf{B}_\beta$ is zero, the intrinsic permeability tensor can now be computed as

$$\mathbf{K}_\beta(\mathbf{x}) = \langle \mathbf{D}_\beta \rangle \tag{A.6}$$

820 In Fig. 14 we plot the spatial variations of K_β^{-1} predicted from the solution of the LCP taking two values of r_0 for two values of $\varepsilon_{\beta\omega}$. In addition, in the same figure, we plot those predictions
822 obtained from filtering the PSS, an extension of the Carman-Kozeny (CK) equation, a linear function and a step-jump function (Ochoa-Tapia & Whitaker, 1995b; Angot, 1999; Goyeau et al.,

2003; Valdés-Parada et al., 2007a). Here the extension of the CK equation is obtained when the value of $\varepsilon_{\beta\omega}$ is replaced by ε_{β}. It is interesting to note that the permeability predictions obtained from the solution of the LCP are the closest to those obtained from the PSS. On the contrary, the predictions using the step-jump function exhibit the largest deviations from those of the PSS. Finally, the predictions using the extension of the CK equation and the linear function also exhibit deviations and they are more close to those obtained from using the step-jump function. Therefore, until better methodologies are found, and when the PSS is not possible, the LCP can be the best alternative available to predict the permeability in the inter-region.

Highlights

- The one-domain approach (ODA), with the generalized transport equations obtained with the volume averaging method, can accurately describe the momentum transport in a free fluid/porous medium system.

- The average momentum eqution must include the well-known Brinkman's correction to Darcy's law but also a second Brinkman's correction and a position-dependent permeability tensor.

- The ODA exactly describes the velocity profiles everywhere in a free fluid/porous medium system even if the micro structure of porous medium changes near the porous medium boundaries.

- The position-dependent permeability tensor is computed from both pore-scale simulations and the solution of the corresponding local closure problem in a representative domain of the free fluid/porous medium boundary.

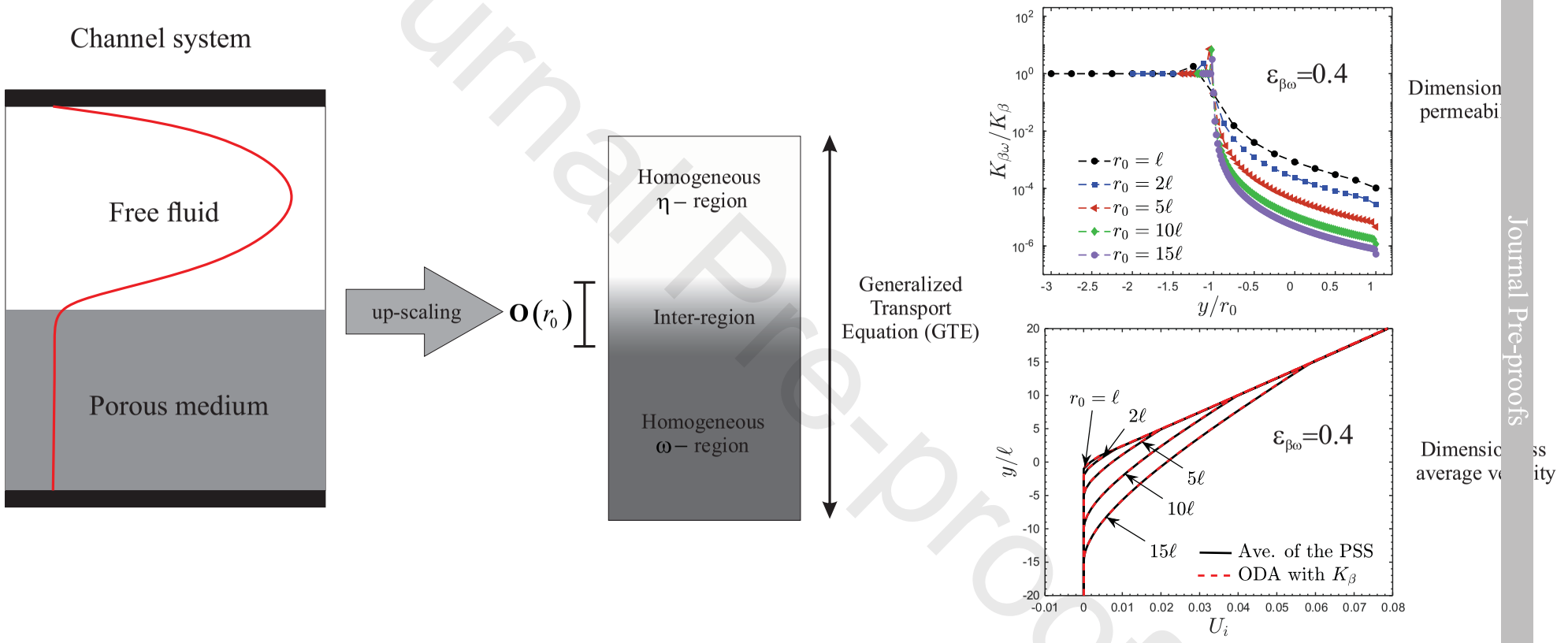

Dimension
permeabi

Dimensio ss
average ve ity

Declaration of interests

- The authors declare that they have no known competing financial interests or personal relationships that could have appeared to influence the work reported in this paper.